CONFIDENTIAL CLASSIFIED COPY
X 62 64229 93
RM E57A24

NACA RM E57A24

Atic 326686

NACA RESEARCH MEMORANDUM

CASE FILE COPY

EVALUATION OF SEVERAL RAM-JET COMBUSTOR CONFIGURATIONS USING PENTABORANE FUEL

By John W. Sheldon and A. J. Cervenka

Lewis Flight Propulsion Laboratory
Cleveland, Ohio

CLASSIFICATION CHANGED TO DECLASSIFIED AUTHORITY #50 4/12/61

DOWNGRADED AT 12 YEAR INTERVALS; NOT AUTOMATICALLY DECLASSIFIED. DOD DIR 5200.10

CLASSIFIED DOCUMENT
This material contains information affecting the National Defense of the United States within the meaning of the espionage laws, Title 18, U.S.C., Secs. 793 and 794, the transmission or revelation of which in any manner to an unauthorized person is prohibited by law.

NATIONAL ADVISORY COMMITTEE FOR AERONAUTICS

WASHINGTON

April 1, 1957

APR 4 1957

CONFIDENTIAL

DECLASSIFIED

NATIONAL ADVISORY COMMITTEE FOR AERONAUTICS

RESEARCH MEMORANDUM

EVALUATION OF SEVERAL RAM-JET COMBUSTOR CONFIGURATIONS USING PENTABORANE FUEL

By John W. Sheldon and A. J. Cervenka

4232

CR-1

SUMMARY

AT

Several combustor configurations of a $9\frac{3}{4}$-inch-diameter ram-jet engine were investigated to determine if the length of the engine could be reduced. It appears feasible that a highly reactive fuel such as pentaborane can be burned in the low subsonic region of the diffuser, thus reducing the engine length by eliminating part of the diffuser. A satisfactory combustor design consisted simply of locating the fuel injectors and pilot at the downstream end of the shortened centerbody. The fuel injector, located in a uniform high-velocity flow region, injected fuel normal to the airstream. The injectors were insulated to prevent thermal decomposition of the fuel.

Combustion efficiencies greater than 90 percent were obtained at equivalence ratios from 0.50 to 0.85. High efficiencies were also obtained at lower equivalence ratios by sizing the injectors for lower fuel flows. JA

INTRODUCTION

The possibility of improving the range of jet-propelled aircraft by using high-energy fuels is being investigated at the NACA Lewis laboratory. Aerodynamic analysis has shown that a ram-jet-powered missile of a given weight has a range potential up to 50 percent greater with pentaborane fuel than with hydrocarbon fuel (ref. 1). It may be possible to further increase the potential of pentaborane fuel by making use of its high reactivity in order to reduce engine size and weight.

One of the possible methods for reducing engine weight is to shorten the subsonic diffuser. The method most frequently used to reduce diffuser length is to increase the divergence angle; but this often causes flow separation, which, in turn, results in nonuniform airflows and fuel-air mixtures. Poor temperature profiles caused by flow distortion reduce thrust and may also produce hot spots in the combustor, and thus induce engine failure.

An alternate way to reduce the diffuser length and avoid the problems of airflow distortion is to eliminate a section of the low Mach number diffuser. This means that the combustor-inlet velocity will be increased and, hence, the combustor pressure drop due to momentum change will be increased. This method therefore appears more promising at the higher flight Mach numbers, where the loss in total pressure has little effect compared with the savings in engine length and improved engine efficiency. For example, the over-all efficiency of a ram-jet engine at a flight Mach number of 4.0 is dropped from 38 to 37 percent (ref. 2) as the combustor pressure is decreased by 1 kinetic head ($\Delta p/q = 1.0$). (Symbols are defined in appendix A.) At a flight Mach number of 1.5, engine efficiency decreases from 17 to 16 percent (ref. 2) for the same loss in combustor pressure.

When conventional hydrocarbon fuels are used, it is necessary to diffuse to low velocities in order to have adequate combustion stability. However, with a highly reactive fuel such as pentaborane, it appears advantageous to reduce the amount of subsonic diffusion, thus initiating combustion where the Mach number is relatively high.

The main objective of this program was to investigate the possibility of reducing the length of an engine by burning pentaborane fuel in the low subsonic region of the diffuser, thus eliminating part of the subsonic diffuser. This system has the advantage of a uniform high-velocity airflow at the fuel-injection station in addition to being shorter. These advantages must be weighed against the reduction in diffuser pressure recovery.

Secondary objectives were to check the performance of a convergent-divergent exhaust nozzle for the engine configuration of reference 3 and to obtain higher combustion efficiencies than are reported in reference 4 at high fuel-air ratios.

The results of experiments with a $9\frac{3}{4}$-inch ram-jet engine operated as a connected pipe are reported herein. Tests were conducted at an inlet-air pressure of 1 ± 0.2 atmosphere, a temperature of 220° F, and a combustor-inlet Mach number range of 0.13 to 0.20 based on the maximum combustor cross-sectional area. The fuel used was liquid pentaborane. Because of the limited supply of fuel, all tests were of short duration, the entire program consuming 43.8 pounds of fuel. The design variables investigated were diffuser and fuel-injector geometries.

APPARATUS AND PROCEDURE

Ram-Jet-Engine Installation

The engine installation shown in figure 1 combines the simplicity of connected-pipe operation with the advantages of free-jet supersonic-

DECLASSIFIED

flight simulation. As can be seen in this drawing, the system is essentially a connected-pipe facility with the addition of a supersonic nozzle and ducting to remove the air spilled around the engine.

Both free-jet and connected-pipe tests have been conducted in this facility with another fuel. These tests showed that the two methods of operation gave similar results when the diffuser was operated with supercritical pressure ratios. All tests with pentaborane fuel were made with the connected-pipe operation since this procedure allows shorter-duration runs, thereby consuming less fuel per data point. The spill-air valve was closed for connected-pipe operation, and all the airflow metered by the combustion-air orifice passed through the engine. The flow velocity through the free-jet nozzle was subsonic.

Combustion air was supplied by the laboratory air supply system. Combustion air was metered and throttled before entering the inlet plenum. From the plenum the flow path led through the free-jet nozzle, the engine, and the exhaust plenum, where it was discharged into the altitude exhaust system. Modulation of the motivating airflow to the altitude exhaust ejectors was used to control the pressure level in the engine. The fuel system was identical to that of reference 4 except for the injectors.

Engine Configurations

A sketch of the engine is shown in figure 2. The supersonic diffuser was identical to that used for the engine configuration of reference 3.

Pilot fuel was injected into the centerbody between stations 1 and 2. The pilot air was furnished by recirculation of part of the main airflow. The main fuel was injected in the plane of station 2. The combustion chamber extended to station 3; this station was the inlet to the exhaust nozzle.

All configuration variations consisted of changes in the centerbody, the fuel injectors, and the exhaust nozzle. The centerbody extended to station 2, and the combustor was of constant area at the maximum cross-sectional area from station 2 to 3 for all three configurations. A sketch of each configuration is shown in figure 3.

The fuel injectors for configurations A and B were designed for operation at a maximum equivalence ratio of 0.30. The fuel injectors for configuration C were designed for equivalence ratios ranging from 0.40 to 1.00.

The exhaust nozzle for configuration A was a convergent-divergent nozzle designed for use on the engine configuration of reference 3. Configurations B and C had a convergent exhaust nozzle with the same inlet-to throat-area ratio as the nozzle of configuration A. The combustor configuration variations are summarized in table I.

03791284039

All fuel injectors were insulated on the downstream side to prevent fuel decomposition within the injector.

Airflow

The combustion air was measured by an orifice in the combustion air duct. The airflow at this orifice was equal to the airflow through the engine except in the transient test of configuration C. The airflow measured by the orifice and flowing through the choked throttle valve was constant during this run. However, as the engine-inlet total pressure increased with increasing fuel flow, a certain quantity of air was required to increase the air density in the inlet ducts between the throttle valve and the engine inlet. As the time rate of change of inlet pressure decreased, the engine-inlet airflow approached the flow through the throttle valve. If a steady inlet pressure were obtained, the engine-inlet airflow would have equaled the flow through the throttle valve.

4232

Fuel Flow

The fuel-flow rate was recorded continuously as a function of time by means of a rotating-vane flowmeter giving an electric signal to a self-balancing recording potentiometer.

The flow meter was calibrated with water and converted to pentaborane flow by use of a density factor. This calibration was essentially constant for the duration of the investigation.

Thrust Measurement

The total momentum of the exhaust gases at the throat of the convergent exhaust nozzle was measured by the thrust barrel shown in figure 4(a). The reaction B was measured by a strain gage and transmitted to a recorder through the pressure transducer. The strain gage was calibrated by placing a second transducer of known calibration in series with the first and hydraulically loading the system.

Two static pressures in the thrust barrel were also sensed by pressure transducers. These pressures and the thrust-barrel strain-gage force were indicated on a four-channel oscillograph, which recorded data continuously as a function of time. The measured stream thrust F_m may be determined by a momentum balance around the exhaust nozzle and thrust barrel shown in figure 4(b). The resulting expression is

$$F_m = B + p_6(A_4 + A_5) - p_5A_5$$

DECLASSIFIED

Then, the air specific impulse S_a is

$$S_a = \frac{F_m}{w_a}$$

A series of calibration tests were conducted to determine the validity of the preceding equations. A description of these tests is presented in appendix B.

4232

Temperature Profiles

Temperatures were measured by thermocouples at station 3 and recorded on self-balancing potentiometers. Profiles were obtained for configurations A and B at equivalence ratios of 0.10 and 0.24. For configuration A, 16 platinum - platinum-rhodium thermocouples, located in centers of equal areas, were used. For configuration B, 20 chromel-alumel thermocouples, also located in centers of equal areas, were used. Thermocouple radiation corrections were calculated by the method presented in reference 5.

No profiles were obtained for configuration C, since it was run above the maximum fuel-air ratio for which temperatures could be measured without damage to the thermocouples.

Combustion Efficiency

Combustion efficiency was determined over a range of equivalence ratios for each configuration. Equivalence ratio is the metered fuel-air ratio divided by the stoichiometric fuel-air ratio of 0.0765 for pentaborane in air.

The exhaust-gas temperatures at the burner exit for configurations A and B were averaged on a mass-weighted basis, assuming a constant Mach number at the combustor exit and a Mach number of 1.0 at the exhaust-nozzle throat. The combustion efficiency was defined as

$$\eta_B = \frac{\varphi_i}{\varphi_m}$$

where φ_i is the theoretical equivalence ratio, as given by reference 6, required to obtain the measured temperature, and φ_m is determined from the measured fuel-air ratio. The theoretical curves of combustion temperature against equivalence ratio for various inlet-air temperatures are reprinted from reference 6 (fig. 1(g)) in figure 5(a).

03T912A1030

Thrust-barrel data were taken for configurations B and C to allow determination of air specific impulse at the throat of the convergent exhaust nozzle for several equivalence ratios. From specific-impulse data, theoretical values of equivalence ratio φ_i were obtained from reference 6. Combustion efficiency was again obtained from the preceding equation. The theoretical curve of air specific impulse against equivalence ratio for various inlet-air temperatures is reprinted from reference 6 (fig. 3(g)) in figure 5(b).

No efficiency was determined from thrust-barrel data for configuration A because of the poor calibration curve resulting from the convergent-divergent exhaust nozzle. This is discussed in more detail in appendix B.

4232

Combustor Pressure Loss

Combustor pressure-loss coefficient was defined as $(P_1 - P_3)/q_t$. The total pressure at the combustor inlet was calculated from measured values of airflow, static pressure, and temperature at station 1. The combustor-exit total pressure P_3 was obtained by the same procedure at station 3 but with an added complication for configuration C. Since exhaust-gas temperature measurements were impossible with configuration C, because of high exhaust-gas temperatures, the exhaust-gas temperature was calculated from the equivalence ratio and combustion efficiency using values of combustion temperature presented in reference 6 (fig. 5).

Pressure-loss data were obtained with and without burning for the three configurations. Maximum and minimum total-pressure losses were computed as follows: An arbitrary maximum momentum pressure loss was calculated by assuming heat addition at the minimum combustor area until a Mach number of 1.0 was obtained. Any further heat addition was done in the diffuser, maintaining the Mach number of 1.0. The momentum loss of this process, added to the cold-flow loss, was defined as the theoretical maximum combustor pressure loss.

A minimum momentum loss was calculated assuming the flow expanded isentropically from the combustor inlet to the maximum combustor cross-sectional area, after which sufficient heat was added to obtain a Mach number of 1.0 in the exhaust-nozzle throat. This momentum loss added to the cold-flow loss was defined as the theoretical minimum combustor pressure loss.

Experimental Procedure

The combustor operating conditions at which the various configurations were compared were

DECLASSIFIED

Inlet-air static pressure, in. Hg abs	35±6
Inlet-air velocity, ft/sec	230-270
Inlet-air total temperature, °F	220±10

All combustion data were obtained with a Mach number of 1.0 at the exhaust-nozzle throat.

Configurations A and B were operated at steady state over a range of equivalence ratio from 0.10 to 0.27, simulating the free-flight conditions of reference 3. Data for configuration C were obtained for equivalence ratios between 0.42 and 1.00. Most of the data for configuration C was obtained during transient operation because of the high fuel-flow rates required and the low fuel supply. Figure 6 shows the variation of thrust, airflow, combustor-inlet total pressure, fuel flow, and equivalence ratio during the transient run of configuration C. Data necessary to obtain combustion efficiency and combustor pressure loss were obtained for the three configurations. After each run, the engine was disassembled and oxide deposits were photographed.

4232

RESULTS

The three combustor configurations were evaluated on the basis of inlet-air velocity profile, exhaust-gas temperature profiles, combustion efficiency, and total-pressure loss. Little information could be obtained on boron oxide deposits because all tests were of short duration; typical deposits encountered can be seen in figure 7.

Inlet Velocity Profiles

The circumferential and radial velocity distributions measured at stations 1 and 2 for configurations A, B, and C with cold air flow are shown in figures 8 and 9. Configuration A had a uniform circumferential velocity profile at station 1 varying ±5 percent from the mean (fig. 8(a)). At station 2, the velocity varied as much as ±60 percent from the mean (fig. 8(b)).

Configurations B and C had the same diffuser configuration. The velocity profile for these configurations was uniform at both stations 1 and 2 (figs. 9(a) and (b), respectively) as would be expected since constant-flow passage area exists between stations 1 and 2. The variation in circumferential velocity at a given radial position was ±8 percent from the mean.

4232

Exhaust-Gas Temperature Profiles

Exhaust-gas temperatures were measured at the combustor exit, station 3, for configurations A and B. The results with configuration A operating at an equivalence ratio φ of 0.105 are shown in figure 10(a). Maximum-to-minimum temperature variation was 1890° F. Operation at a higher fuel-air ratio (φ = 0.237) with the same configuration raised the exhaust-gas temperature level and reduced the temperature spread to 1470° F, as can be seen in figure 10(b).

The results with configuration B at an equivalence ratio of 0.225 are shown in figure 10(c). For this case, the spread in temperature was 1045° F, approximately two-thirds of the variation with configuration A at the richer condition. It is believed that this improvement in temperature pattern was primarily due to the more uniform airflow at the fuel injectors with configuration B. However, part of the improvement may have resulted from the difference in fuel-injector design. Exhaust-gas temperature data were not obtained with configuration C.

Combustion Efficiency

The combustion-efficiency data with the three configurations over a range of equivalence ratios are presented in figure 11. Combustion efficiency was not calculated from air specific impulse for configuration A because of the poor thrust-barrel calibration with the convergent-divergent exhaust nozzle.

The values of combustion efficiency for configuration A were greater than 100 percent when calculated from temperature data. The probable explanation for this can be found in the badly distorted exhaust-gas-temperature profile, which requires many points of measurement to adequately sample the exhaust stream and a mass-weighting technique to give a true energy measurement. Since the local gas velocities corresponding to each temperature were not measured, a simple mass-weighting analysis based on constant Mach number in the plane of station 3 was used. This fact, together with the limited number of temperature measurements, probably accounts for the erroneous combustion-efficiency data. It can only be conjectured that combustion efficiencies with configuration A were near 100 percent.

Combustion efficiency for configuration B was obtained from temperature data and from air-specific-impulse data. This configuration showed a rapid increase in efficiency with increasing equivalence ratio. A value of about 90 percent was reached at an equivalence ratio less than 0.27. These data were recorded with steady-state engine operation, which required relatively large expenditures of fuel per data point; and the highest equivalence-ratio point shown was not a combustion limit but, rather, was

DECLASSIFIED

an operational limit imposed by fuel shortage. Instrumentation for a transient run was not available at the time of this run. It is probable that higher-equivalence-ratio operation would have resulted in decreasing efficiency because of heavier spray impingement on the walls with the radially directed fuel jets.

Configuration C was designed for operation at higher fuel-air ratios by sizing the fuel orifices for larger flow rates. Wall impingement was minimized by using circumferentially rather than radially directed sprays. Temperature data were not taken because of the high-equivalence-ratio operation. Combustion efficiencies from the air-specific-impulse data with this configuration are shown in figure 11.

Data for the leanest condition (φ = 0.42) were obtained with steady-state engine operation, and the remaining data at higher equivalence ratios were obtained with transient operation in order that more high-equivalence-ratio data could be obtained from the limited quantity of fuel. The two data points shown at an equivalence ratio of 1 do not represent a constant fuel-flow rate, but, by coincidence, the increase in fuel flow matched the increased airflow as the pressure rise in the system decreased.

Combustion efficiency for configuration C was above 90 percent at equivalence ratios from 0.50 to 0.85. Combustion efficiency increased with increasing mixture strength to a peak near 100 percent at an equivalence ratio around 0.6 and then decreased with increased equivalence ratio. The low efficiency at the leanest mixture was believed due to poor fuel atomization at low injection pressures. Although combustion efficiency decreased at mixtures richer than 0.7 equivalence ratio, this configuration gave considerably better performance than did the design of reference 4. This was thought to be primarily due to the fuel-injector design, which was tailored to minimize wall impingement. From these results it appears that at typical ram-jet operating conditions it is possible to select the equivalence ratio for peak combustion efficiency by properly sizing and positioning the fuel injectors.

Combustor Total-Pressure Loss

The total-pressure-loss data for the three configurations are shown in figure 12. The total-pressure-loss coefficient $(P_1 - P_3)/q_t$ is given as a function of combustor total-temperature ratio τ. Theoretical curves of maximum and minimum losses for configuration C are presented in addition to measured losses. The maximum-loss curve represents heat addition in the minimum combustor cross section and in the diffuser at a constant Mach number of 1.0. The minimum-loss curve represents heat addition after the flow has expanded to the maximum combustor cross section. A pressure loss between these curves indicates heat addition between the maximum and

03I4I24J330

minimum combustor cross sections. Similar maximum- and minimum-loss curves may be plotted for configurations A and B but are omitted for clarity. These corresponding curves would be straight lines constructed parallel to those for configuration C and through the cold-flow ($\tau = 1$) points for their respective configurations.

The pressure loss of configuration A was expected to be approximately that predicted by a minimum-flow curve, since the configuration diffuses the flow to a low subsonic velocity before fuel is injected. The measured losses for this configuration fell slightly below the minimum loss, probably because of flow variation from the assumed one-dimensional pattern. Configurations B and C, which inject fuel into the minimum combustor cross-sectional area, had pressure losses between the minimum- and maximum-loss curves, indicating a portion of the heat release occurs before the flow has expanded to the maximum-flow area. It is interesting to note the shift in pressure-loss data for configuration C above the minimum-loss curve with increased temperature ratio. This shift indicates an increased amount of fuel is burned before expansion, with increased combustor temperature ratio.

Exhaust-Nozzle Performance

The convergent-divergent exhaust nozzle of configuration A was designed for an engine configuration similar to that of reference 3. A short nozzle with an abrupt radius at the throat was selected because of ease of adapting this nozzle to the flight engine.

The calibration of this nozzle for use with the thrust barrel (see appendix B) indicated flow separation in the diverging portion. Figure 13 shows, for various nozzle pressure ratios, the variation of measured thrust from ideal thrust calculated from one-dimensional flow relations. These data are similar to those reported in reference 7 for separation in a nozzle of similar geometry.

A convergent nozzle, which gave an excellent thrust-barrel calibration, was used with configurations B and C in order to obtain air-specific-impulse data.

DISCUSSION

The selection of the best combustor configuration for a ram-jet engine depends on the flight conditions. The flight conditions are usually chosen such that the range of a ram-jet-powered missile is at a maximum for a given size and cost. At cruise conditions the range may be expressed as

DECLASSIFIED

$$R = H\eta_e \frac{L}{D} \ln \frac{1}{\frac{W_e}{W_g} + \frac{W_{af}}{W_g} + \frac{W_{pl}}{W_g}}$$

The heating value of the fuel H is a function of the chemical properties of the fuel. Pentaborane increases H about 50 percent over that for hydrocarbon fuels.

With regard to combustor design, the factors that give best range are high combustion efficiency and low pressure drop (these serve to increase η_e in the preceding eq.), and low engine weight (which serves to decrease W_e in the same eq.). The engine efficiency, hence range, is also affected by equivalence ratio. The analysis of reference 2 shows a maximum over-all engine efficiency η_e at a flight Mach number of 4.0 and a combustor-outlet temperature of 3000° to 3500° F. However, the best engine temperature ratio, and, consequently, equivalence ratio, is strongly affected by the particular aircraft design and flight path. The three combustor configurations of this investigation gave high combustion efficiency at several temperature ratios, bracketing the optimum temperature ratios of reference 2. This was accomplished by designing the fuel injectors to produce an even distribution of fuel over the flow cross section and to prevent the fuel spray from impinging on the combustor wall. The results of this investigation indicate that weight savings by shortening the diffuser entailed additional pressure losses (fig. 12). The optimum compromise between engine length (weight) and pressure loss must be determined from a detailed analysis for each flight mission. For certain flight missions, it appears that it is beneficial to burn in the subsonic portion of the diffuser to obtain reduced engine weight at the expense of increased pressure loss.

At high flight Mach numbers, and, consequently, high combustor temperatures, it will be necessary to insulate the fuel injectors, as was done in this investigation, to prevent fuel decomposition within the injectors. Excessive local combustion temperatures at the combustor walls will induce combustor failure. In order to avoid these high local temperatures, fuel was injected and burned in the subsonic diffuser where a high uniform airflow existed.

CONCLUSIONS

Reducing engine length by eliminating part of the subsonic diffuser appears feasible if a highly reactive fuel such as pentaborane can be burned in the low subsonic region of the diffuser. A satisfactory combustor design consisted of a fuel injector and a pilot located at the downstream end of the shortened centerbody.

03712241230

With one fuel-injector design, combustion efficiencies greater than 90 percent were obtained at equivalence ratios ranging from 0.50 to 0.85. High efficiencies were obtained at leaner mixtures with another injector which was sized for lower fuel flows.

Excellent combustor performance was obtained when the following fuel-injector design principles were followed: (1) The fuel injectors were located in a uniform high-velocity airstream, (2) the fuel was sprayed normal to the airstream but did not impinge upon the combustor wall, (3) multiple-point injection was used up to the limits of tolerable flow blockage, and (4) the fuel injectors were insulated against overheating.

4232

Lewis Flight Propulsion Laboratory
National Advisory Committee for Aeronautics
Cleveland, Ohio, January 25, 1957

DECLASSIFIED

4232

APPENDIX A

SYMBOLS

A	cross-sectional area, sq ft
B	thrust-barrel reaction force, lb
F	stream thrust, lb
H	heating value of fuel, Btu/lb
L/D	lift-drag ratio
m	mass flow, slugs/sec
P	total or stagnation pressure, lb/sq ft abs
p	static pressure, lb/sq ft abs
q	dynamic pressure, lb/sq ft abs
R	range
S_a	air specific impulse, lb-sec/(lb air)
T	total or stagnation temperature, ^{o}R
W	weight flow, lb/sec
W_{af}	weight of air frame
W_e	weight of engine
W_g	gross weight
W_{pl}	weight of payload
η_B	combustion efficiency
η_e	over-all engine efficiency
τ	total-temperature ratio, T_3/T_1
φ	equivalence ratio, ratio of actual fuel-air ratio to stoichiometric fuel-air ratio

03712241030

Subscripts:

a	air
f	fuel
i	ideal, calculated from one-dimensional flow relations
m	measured
t	based on isentropic expansion from station 1 to total cross section
1	subsonic diffuser entrance
2	fuel-injection station
3	combustor exit
4	exhaust-nozzle exit
5	thrust-barrel diffuser-entrance annulus
6	exhaust plenum

4232

DECLASSIFIED

4232

APPENDIX B

THRUST-BARREL CALIBRATION

The thrust barrel was calibrated by flowing metered quantities of air through the engine and the exhaust nozzle. The stream momentum, computed assuming idealized one-dimensional-flow relations, was compared with the measured stream momentum F_m. The two methods of momentum determination did not agree using the covergent-divergent exhaust nozzle of configuration A (fig. 14(a)). This deviation was attributed to flow separation in the divergent portion of the nozzle. The same calibration was made using the convergent nozzle of configurations B and C, and an agreement was obtained (fig. 14(b)) that was within the accuracy of the instrumentation.

During the transient portion of the test of configuration C, an error in the recording of p_5 occurred because of malfunction of the fast-response pressure-sensing device. As shown in figure 15, p_5 was found by a calibration of p_5 against p_6, obtained by plotting these pressures from previous burning runs. The pressures p_5 and p_6 were indicated on manometers for the steady-state point of the run of configuration C and are also plotted in figure 15. The steady-state data point agrees with the curve of previous runs, thus indicating the method of determining p_5 is reasonably good although quite indirect.

REFERENCES

1. Olson, Walter T., and Gibbons, Louis C.: Status of Combustion Research on High-Energy Fuels for Ram Jets. NACA RM E51D23, 1951.

2. Weber, Richard J., and Luidens, Rodger W.: Analysis of Ram-Jet Engine Performance Including Effects of Component Changes. NACA RM E56D20, 1956.

3. Disher, John H., and Jones, Merle L.: Flight Investigation of Pentaborane in 9.75-Inch-Diameter Ram-Jet Engine with Downstream Fuel Injection. NACA RM E55G01, 1957.

4. Fivel, Herschel J., Tower, Leonard K., and Gibbs, James B.: Pentaborane Combustion Performance in 9.75-Inch-Diameter Ram-Jet Engine in Connected-Pipe Altitude Facility. NACA RM E54I16, 1957.

03712241230

5. Scadron, Marvin D., and Warshawsky, Isidore: Experimental Determination of Time Constants and Nusselt Numbers for Bare-Wire Thermocouples in High-Velocity Air Streams and Analytic Approximation of Conduction and Radiation Errors. NACA TN 2599, 1952.

6. Tower, Leonard K.: Analytic Evaluation of Effect of Inlet-Air Temperature and Combustion Pressure on Combustion Performance of Boron Slurries and Blends of Pentaborane in Octane-1. NACA RM E55A31, 1955.

7. Streiff, M. L.: Exit-Nozzle Design. Ramjet Technology, ch. 13. Appl. Phys. Lab., The Johns Hopkins Univ., 1953. (Contract NOrd 7386 with Bur. Ord., Dept. Navy.)

4232

DECLASSIFIED

TABLE I. - COMBUSTOR CONFIGURATIONS

Configuration	Centerbody between stations 1 and 2	Fuel injectors	Percent of total cross section blocked at station 2 by -	
			Centerbody	Fuel injector
A	$6\frac{1}{8}$" O.D. tapering to 4" O.D.	Eight radial spokes. Forty-eight 0.026-in.-diam. orifices spraying normal to airstream; six equally spaced orifices per injector.	18.0	11.6
B	Constant $6\frac{1}{8}$" O.D.	Octagon ring located in center of equal area. Forty 0.026-in.-diam. orifices equally spaced injecting normal to airstream.	41.0	6.4
C	Constant $6\frac{1}{8}$" O.D.	Sixteen radial spokes. Eighty 0.036-in.-diam. orifices spraying normal to airstream from centers of equal area; orifices are drilled at 79° angle to injector axis, angling the fuel spray away from combustor wall.	41.0	4.0

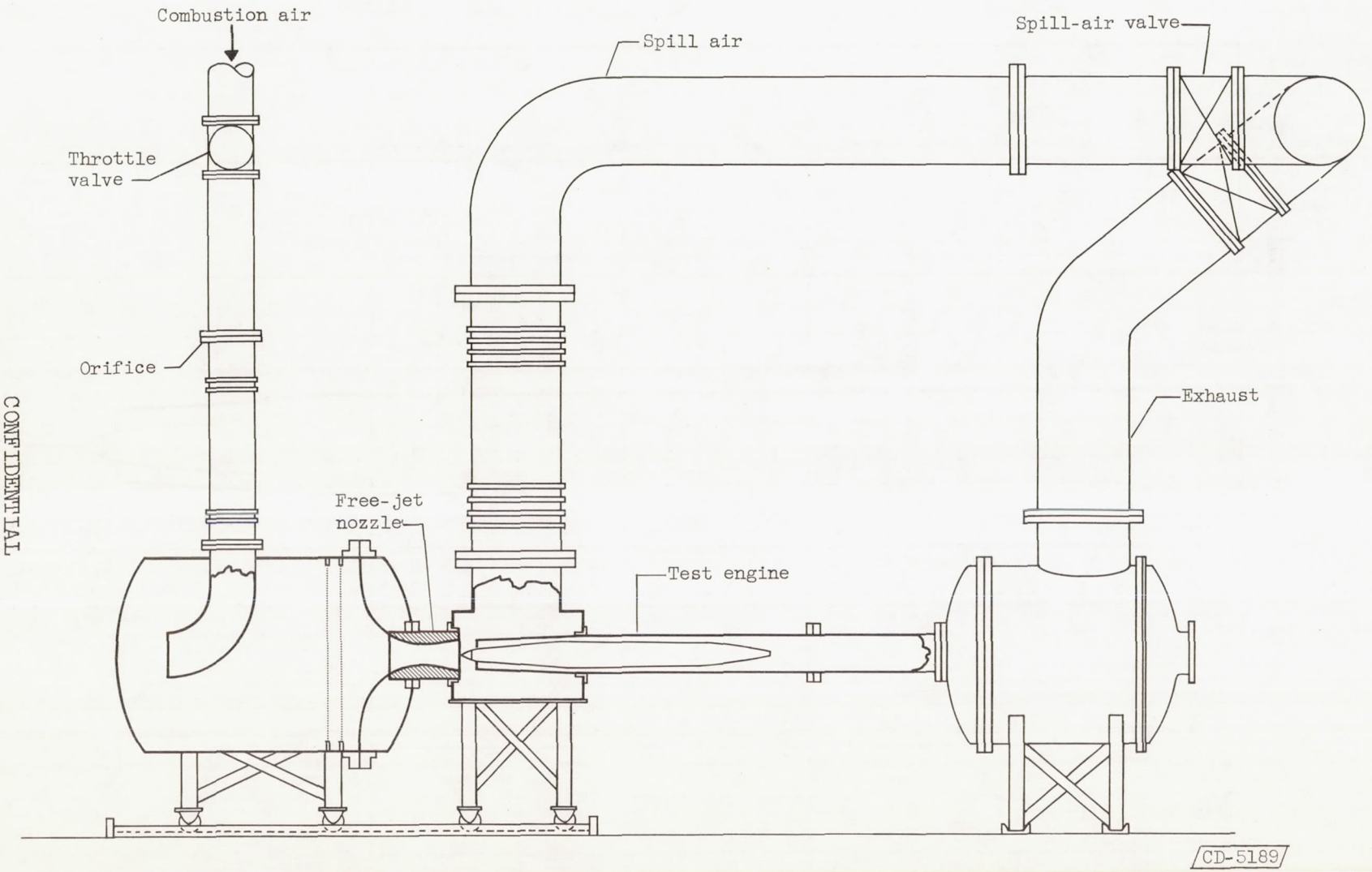


Figure 1. - Installation of ram-jet engine in free-jet test facility.

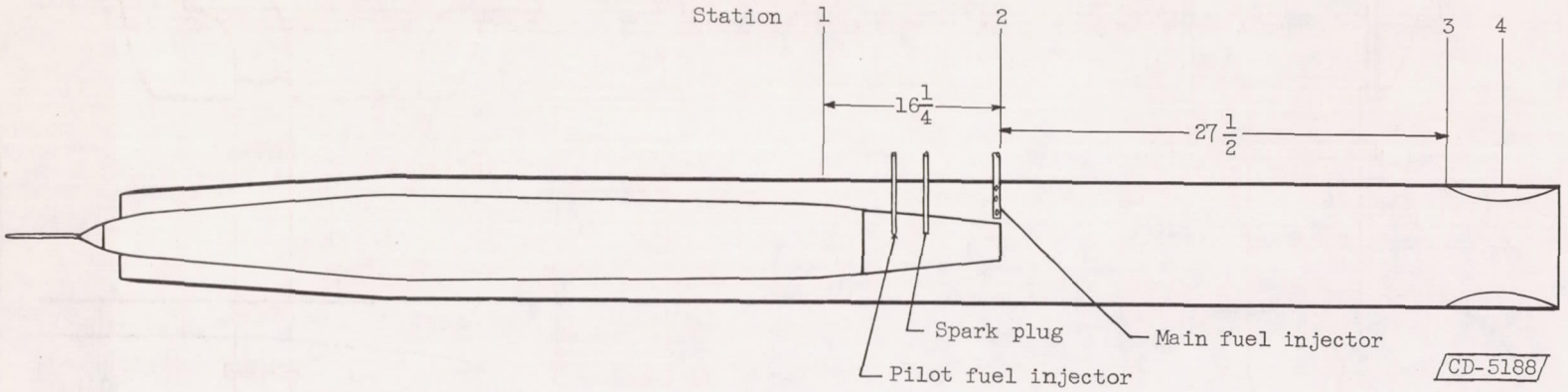
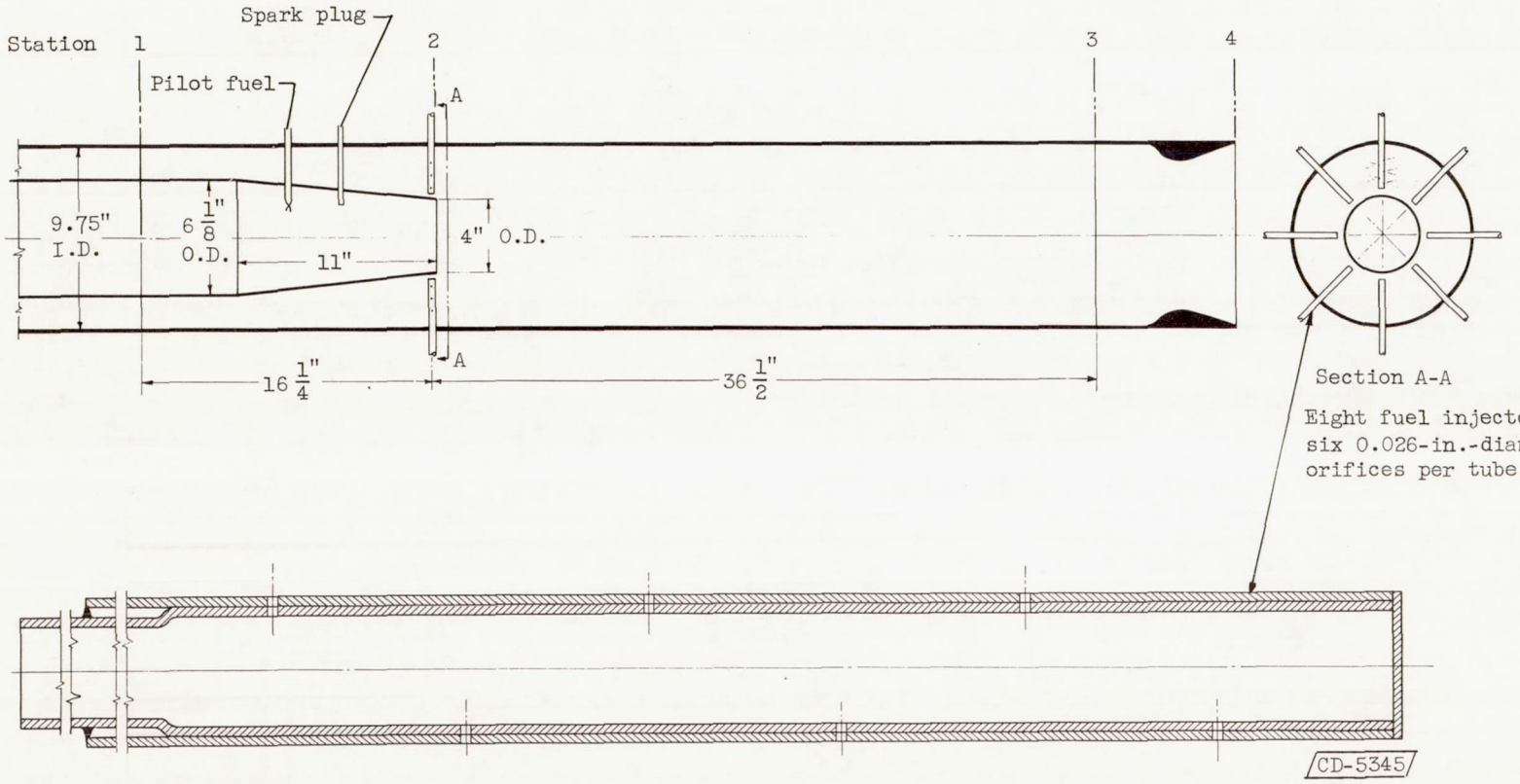
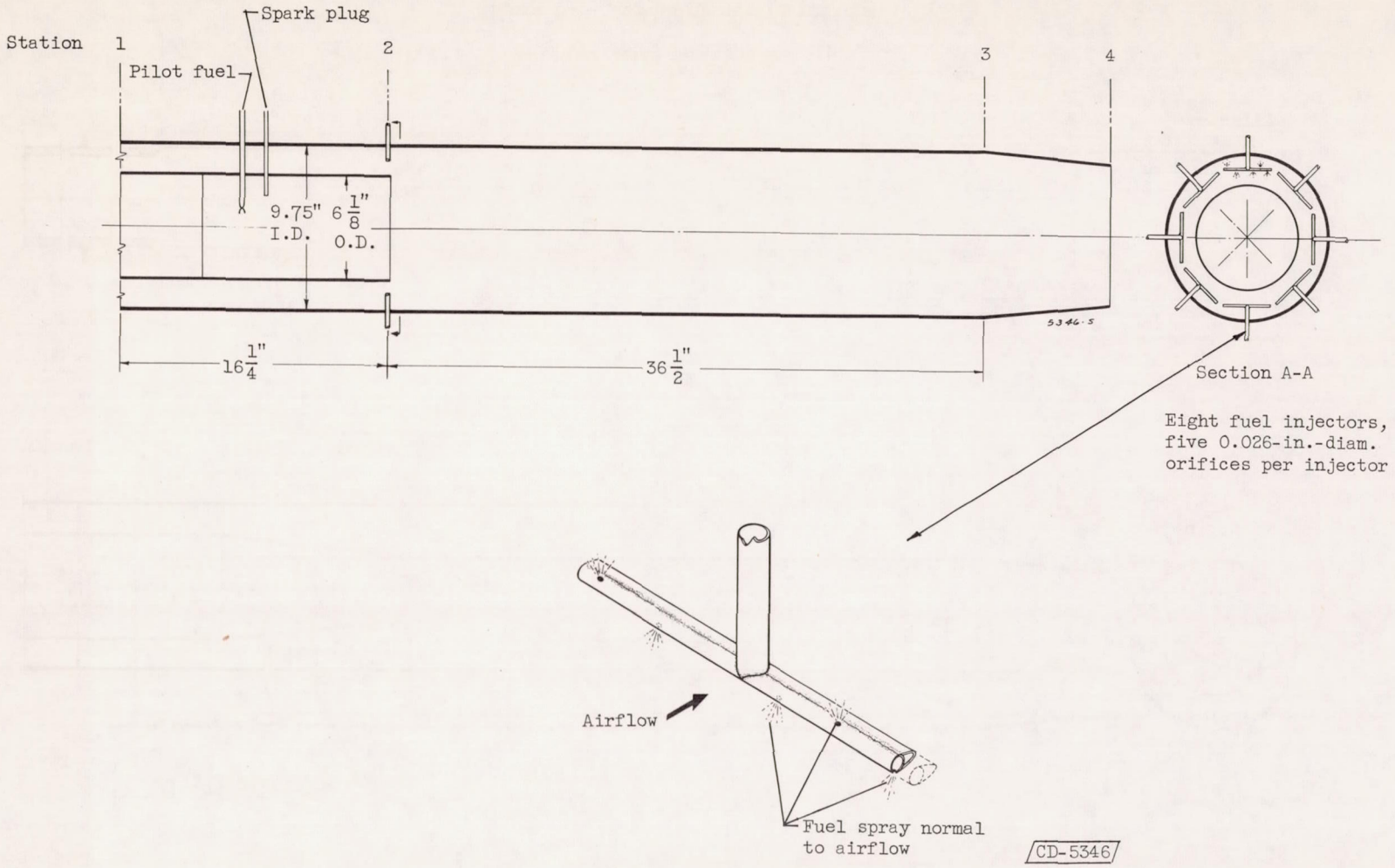


Figure 2. - $9\frac{3}{4}$ -Inch-diameter ram-jet engine. (Dimensions are in inches.)



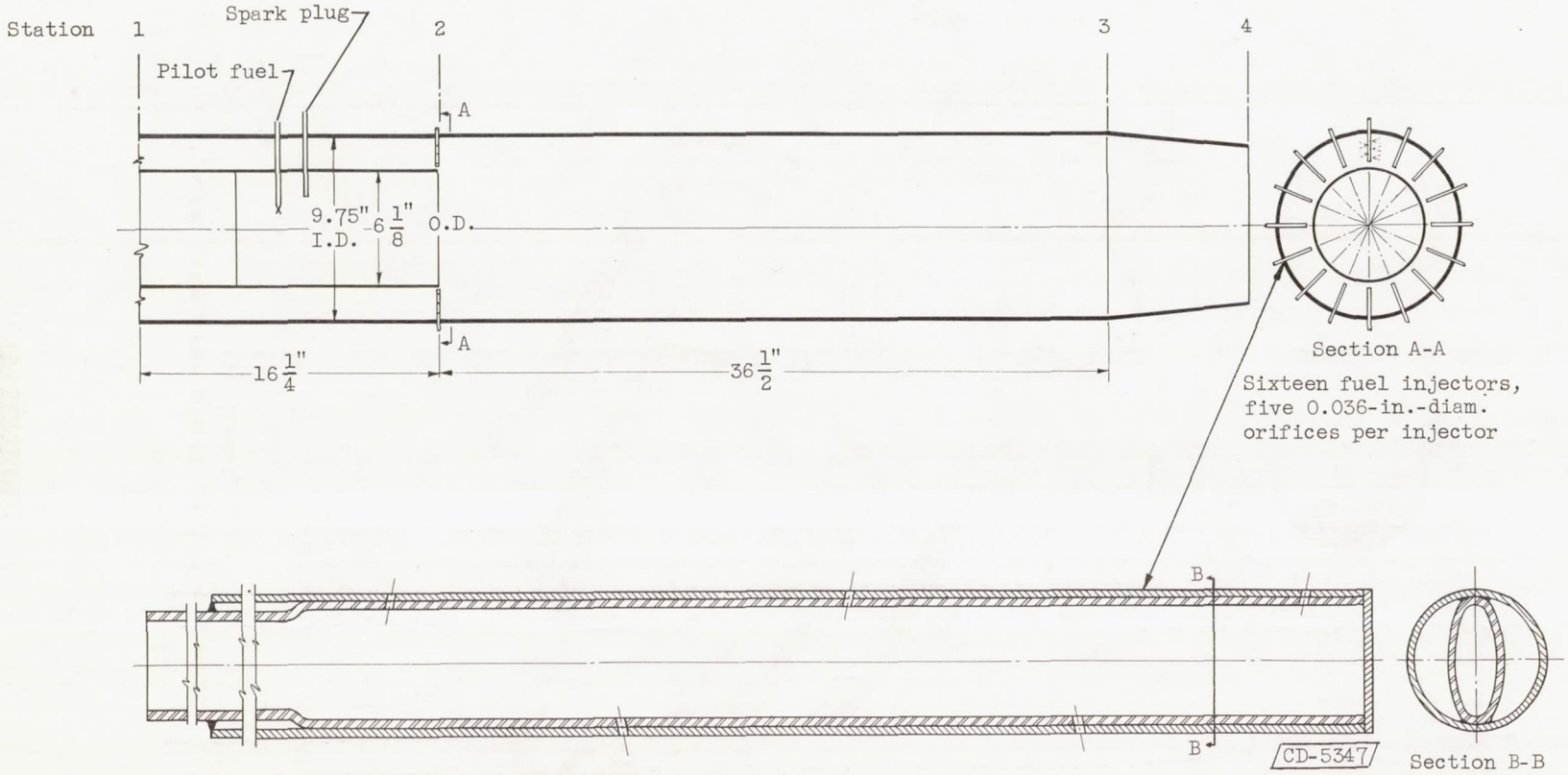
(a) Configuration A.

Figure 3. - Combustor configurations.



(b) Configuration B.

Figure 3. - Continued. Combustor configurations.



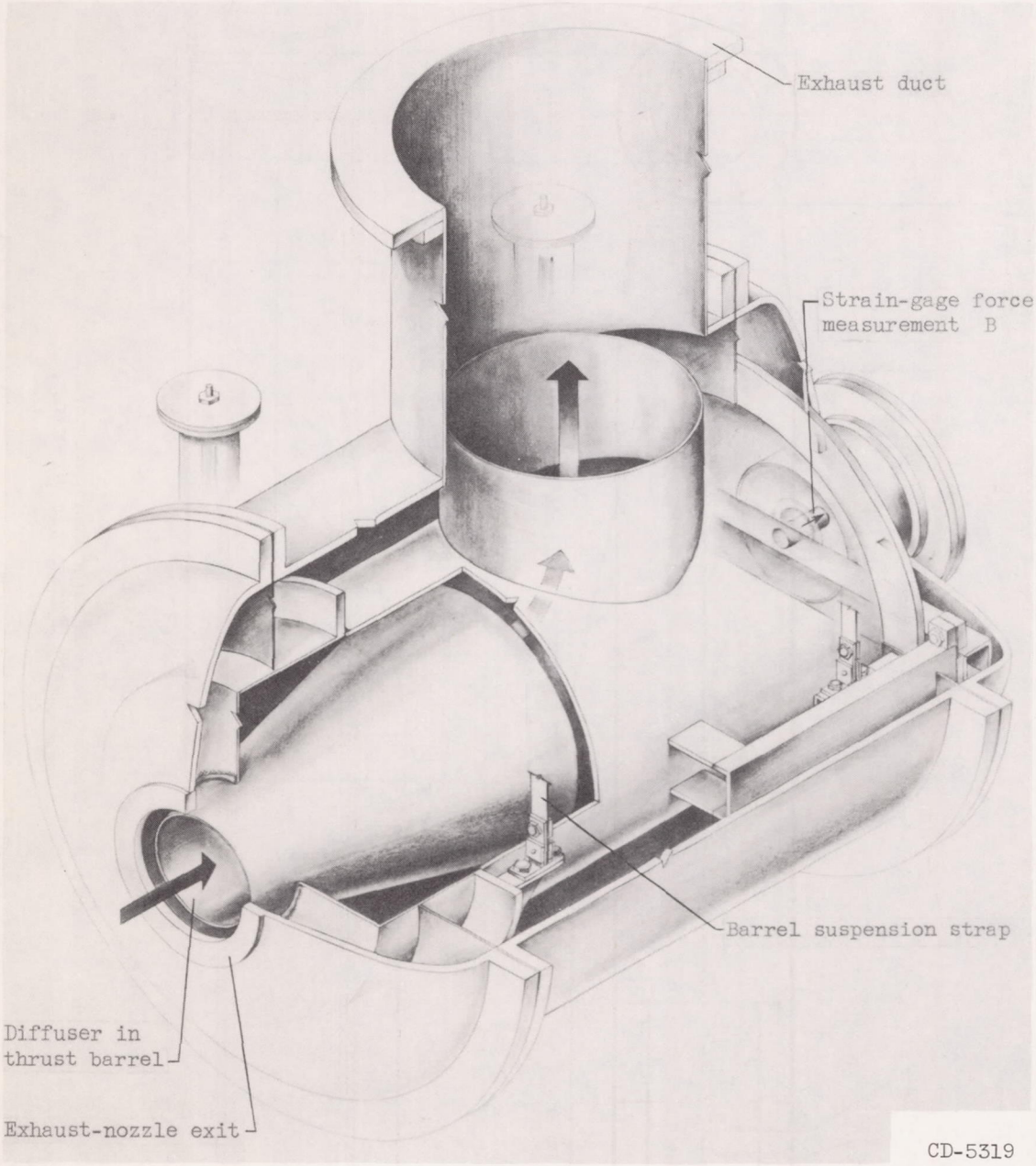
(c) Configuration C.

Figure 3. - Concluded. Combustor configurations.

CONFIDENTIAL

DECLASSIFIED

4232



(a) Cutaway view.

Figure 4. - Exhaust plenum and thrust barrel.

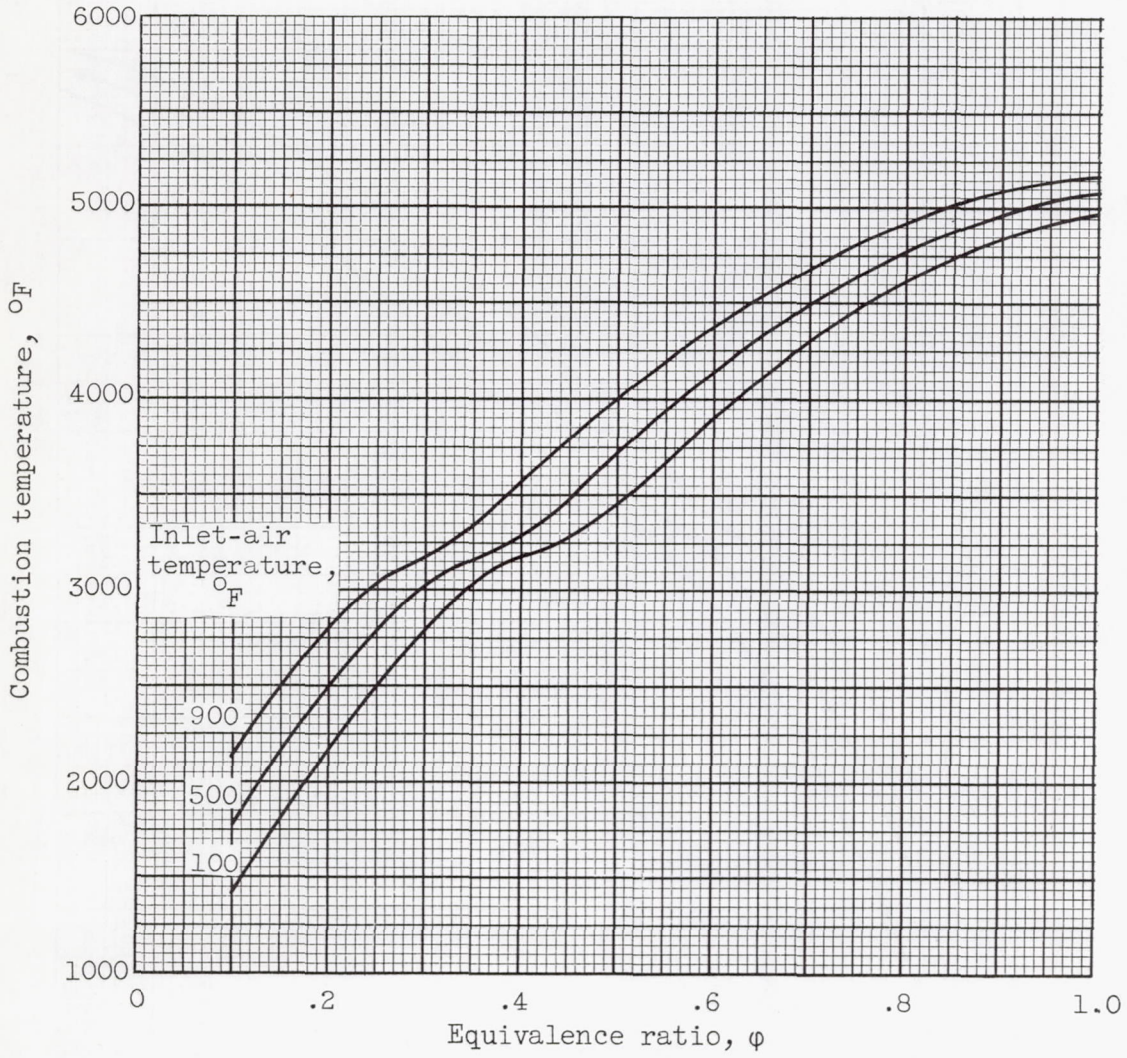
(b) Schematic drawing.

Figure 4. - Concluded. Exhaust plenum and thrust barrel.

DECLASSIFIED

4232

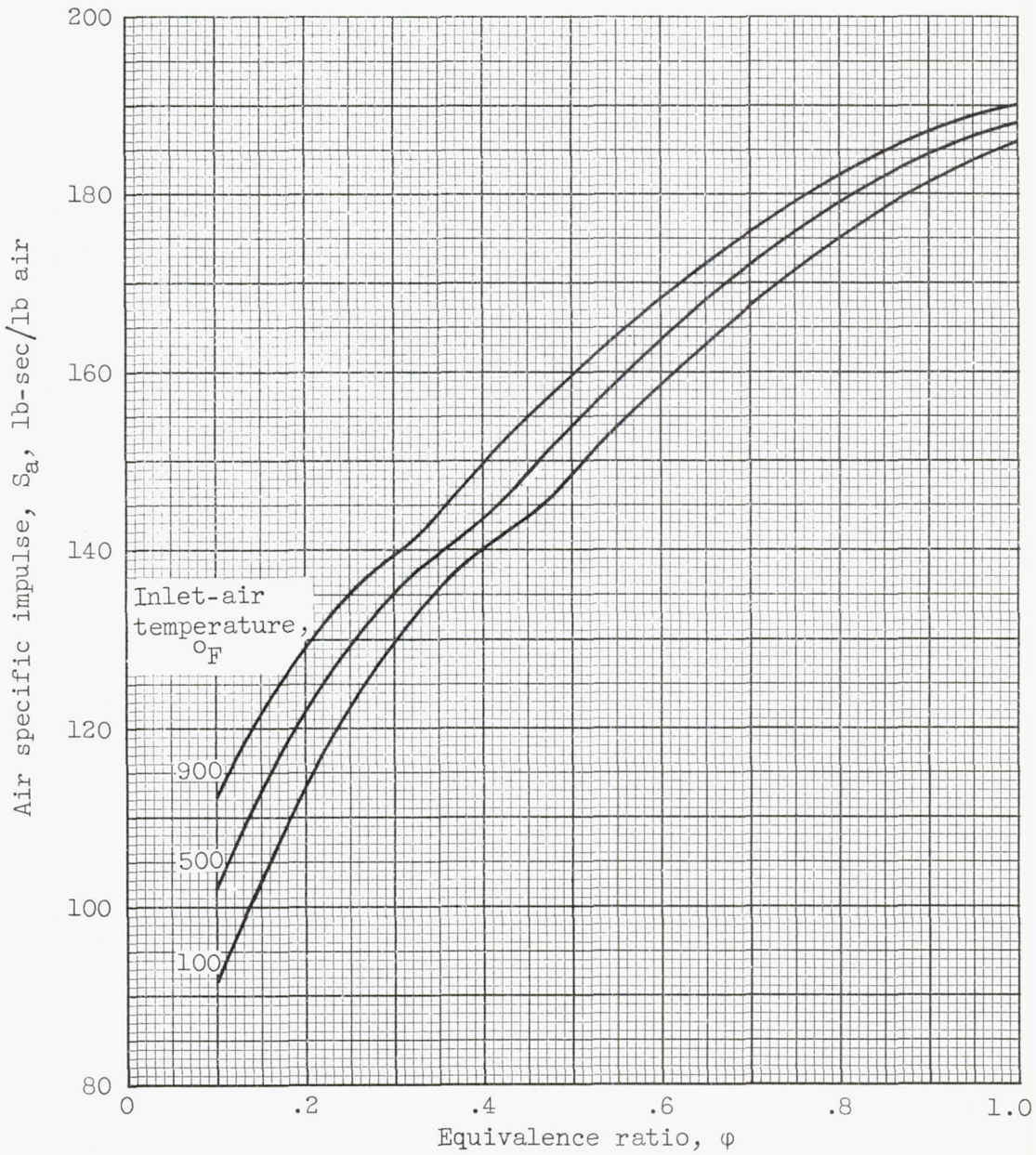
CR-4



(a) Combustion temperature (ref. 6, fig. 1(g)).

Figure 5. - Theoretical effect of inlet-air temperature and equivalence ratio on combustion performance.

4232



(b) Air specific impulse (ref. 6, fig. 3(g)).

Figure 5. - Concluded. Theoretical effect of inlet-air temperature and equivalence ratio on combustion performance.

DECLASSIFIED

CR-4 back 4232

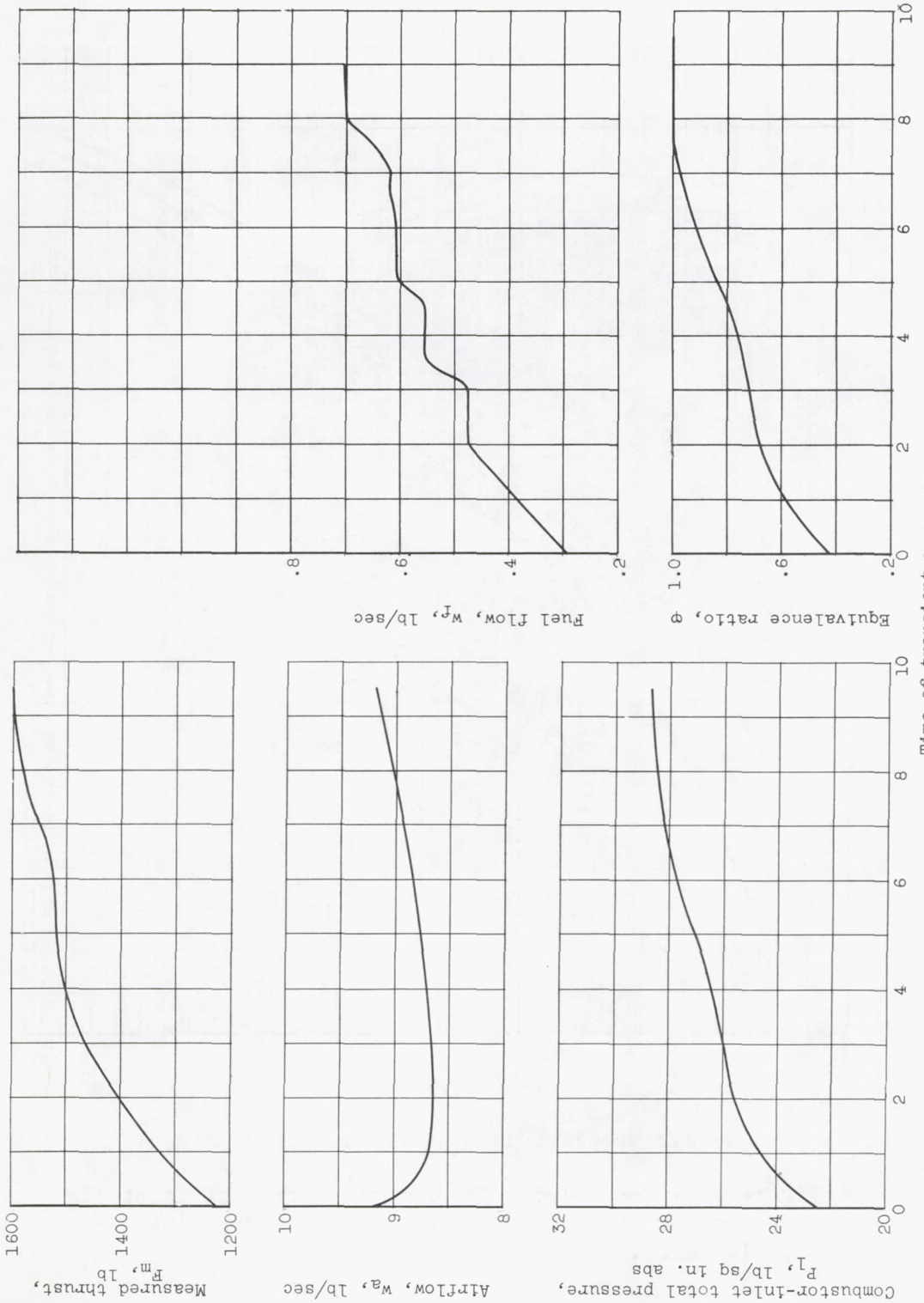
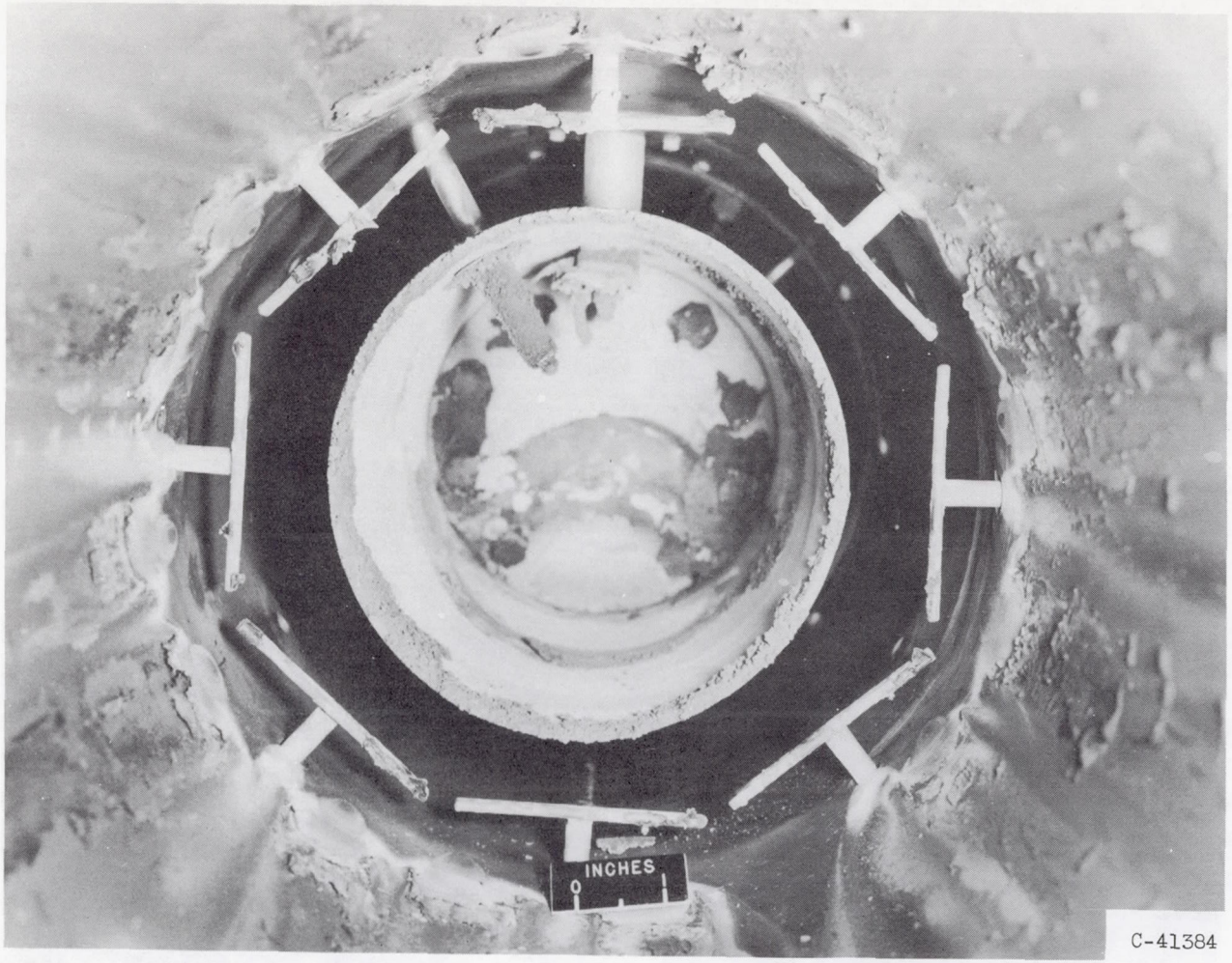


Figure 6. - Transient run of configuration C.

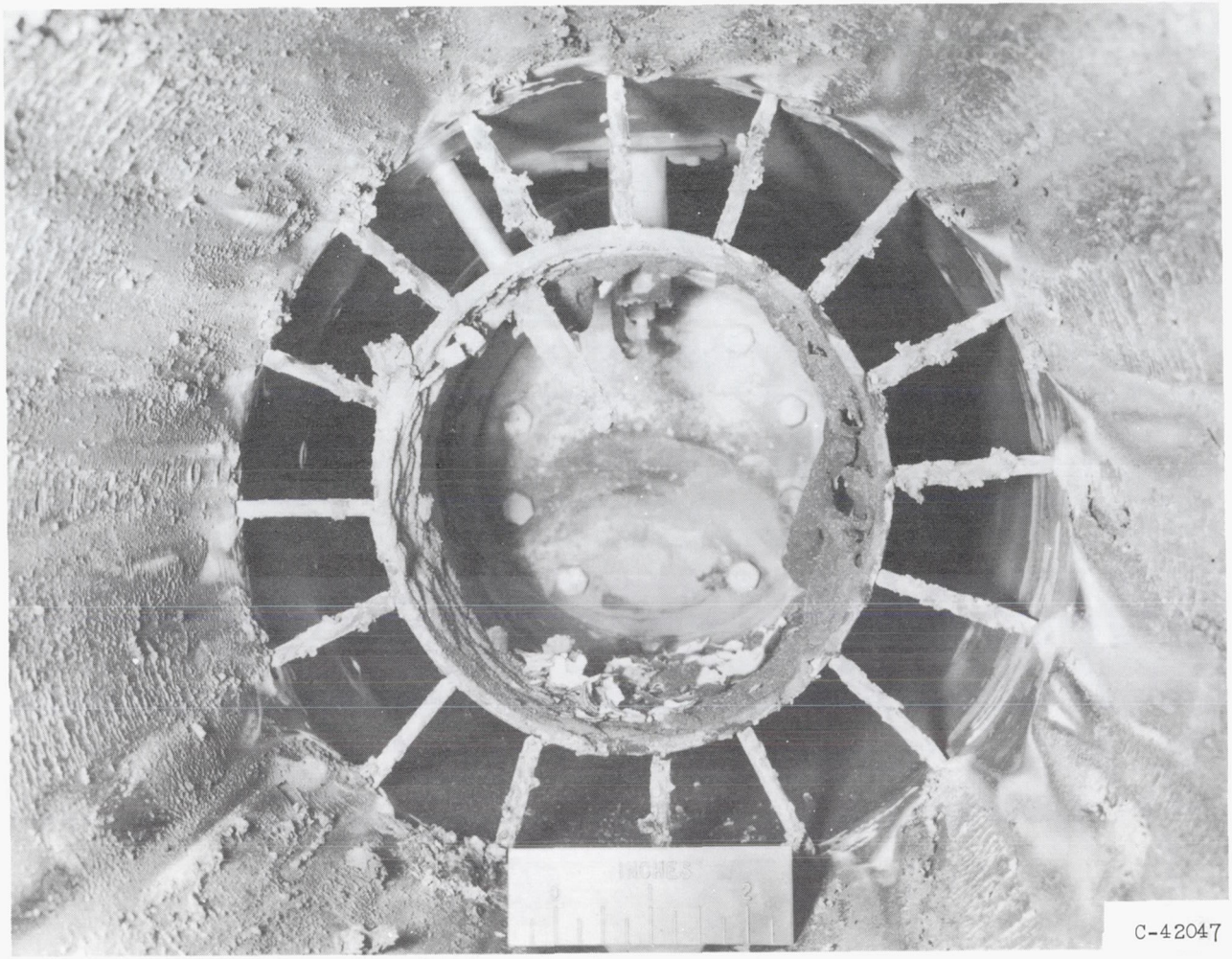
(a) Configuration A; operating time, approximately 30 seconds; equivalence ratios, 0.10 to 0.22.

Figure 7. - Typical oxide products viewed downstream of fuel injector.



(b) Configuration B; operating time, approximately 30 seconds; equivalence ratios, 0.12 to 0.26.

Figure 7. - Continued. Typical oxide products viewed downstream of fuel injector.

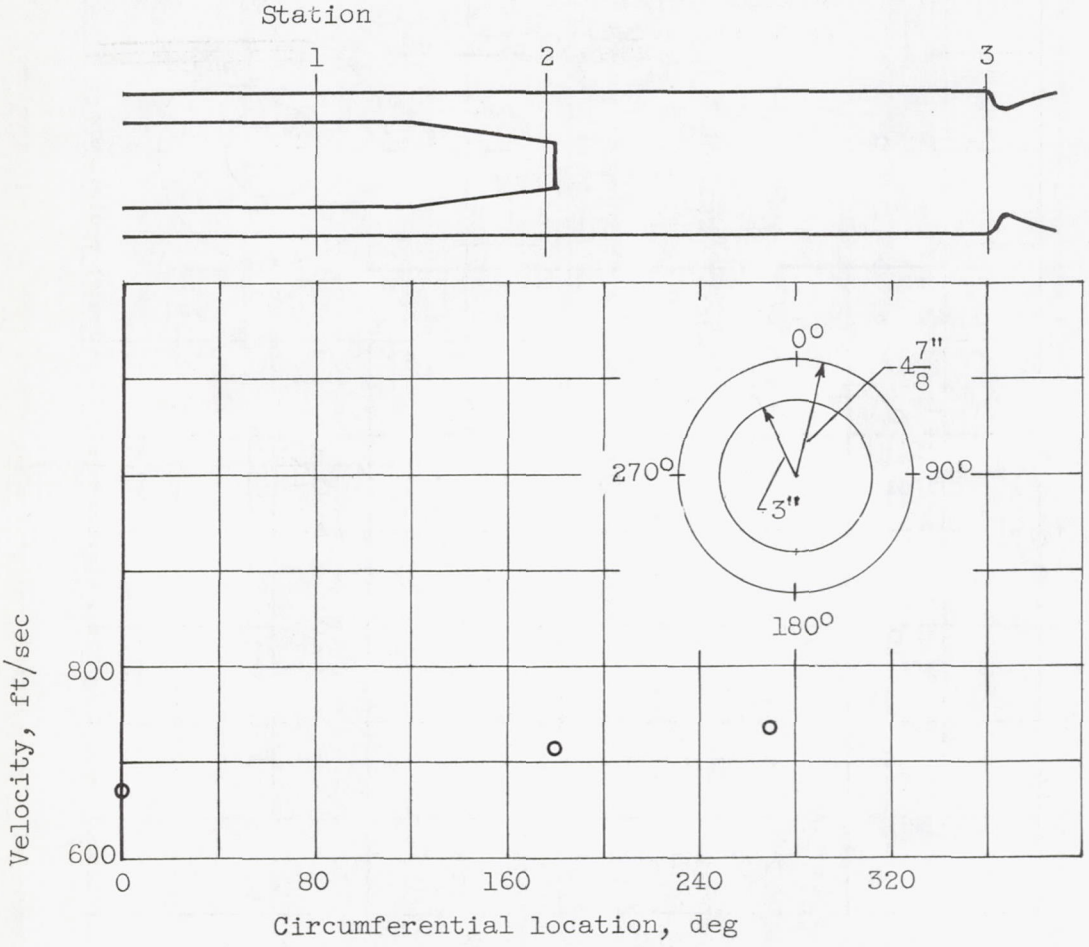


(c) Configuration C; operating time, approximately 10 seconds; equivalence ratios, 0.42 to 1.00.

Figure 7. - Concluded. Typical oxide products viewed downstream of fuel injector.

DECLASSIFIED

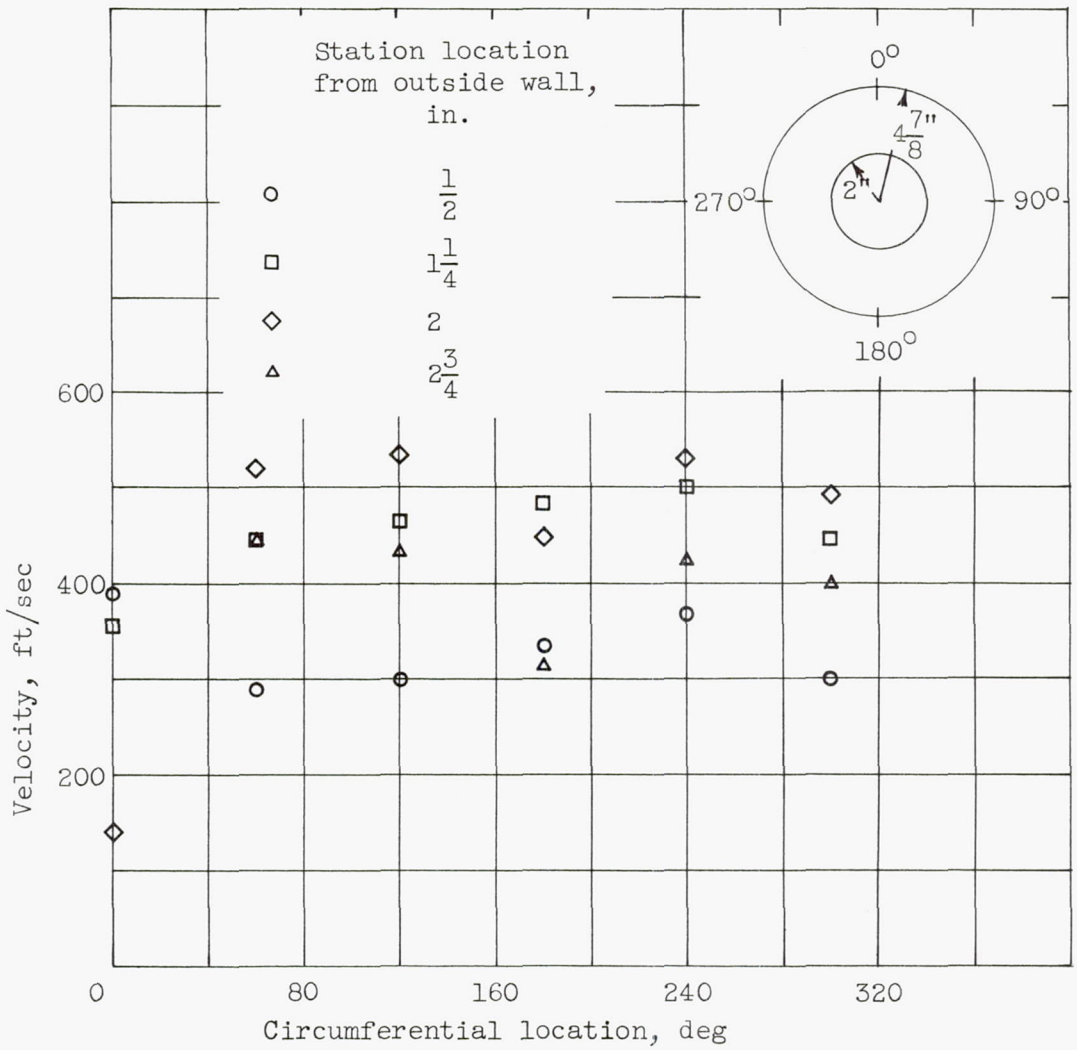
4232



(a) Station 1 ($\frac{7}{8}$ in. from outside wall).

Figure 8. - Combustor-inlet circumferential velocity profiles for configuration A with no combustion. Combustor-inlet static pressure, 35±4 inches of mercury absolute.

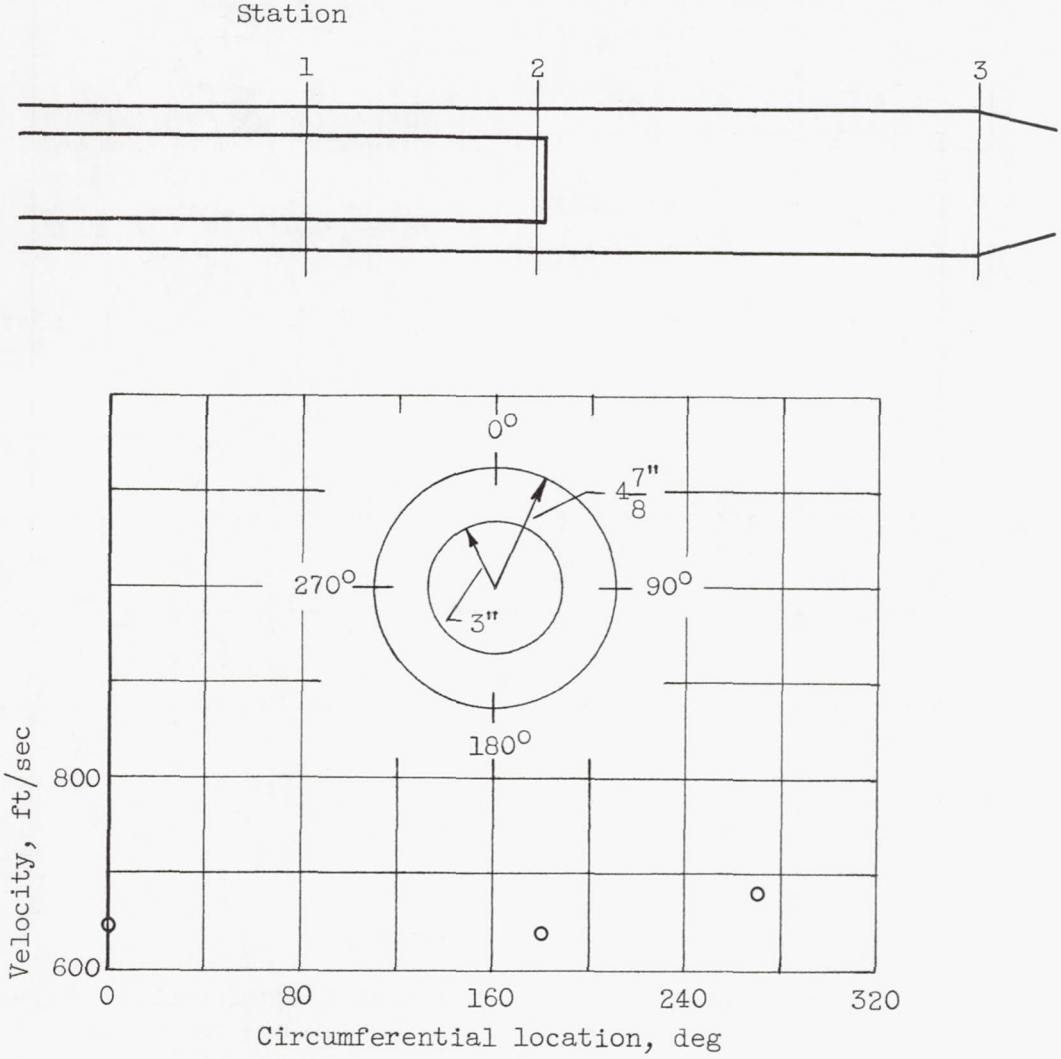
4232



(b) Station 2.

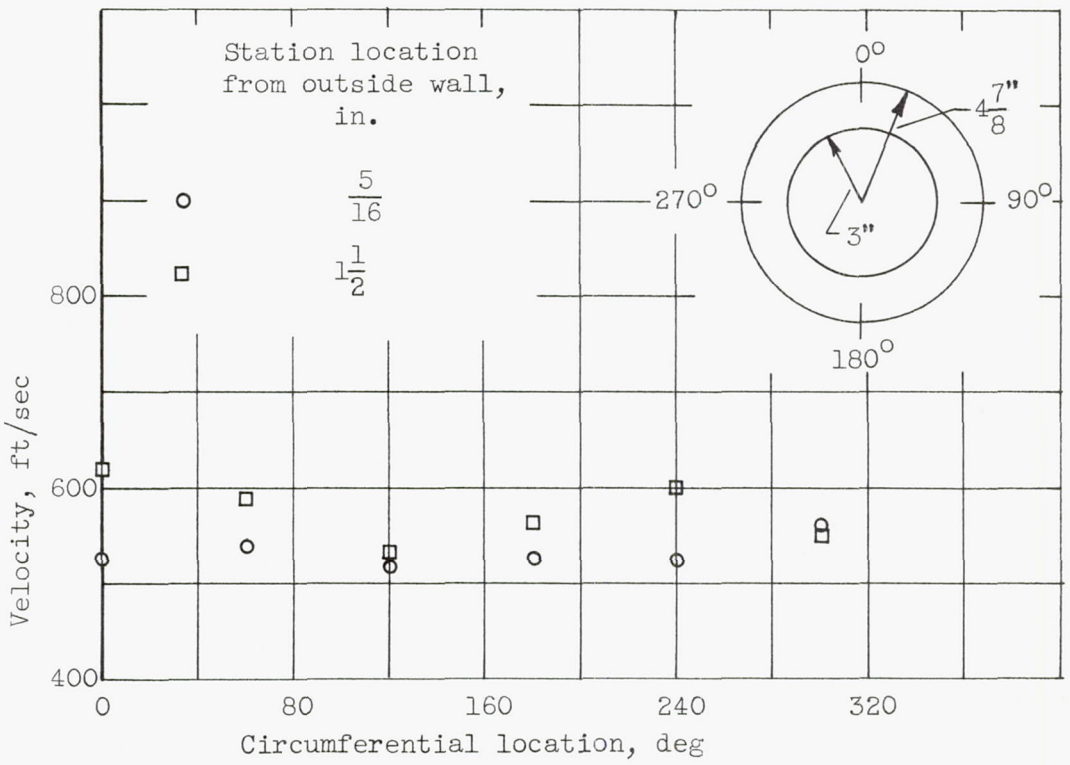
Figure 8. - Concluded. Combustor-inlet circumferential velocity profiles for configuration A with no combustion. Combustor-inlet static pressure, 35±6 inches of mercury absolute.

DECLASSIFIED



(a) Station 1 ($\frac{7}{8}$ in. from outside wall).

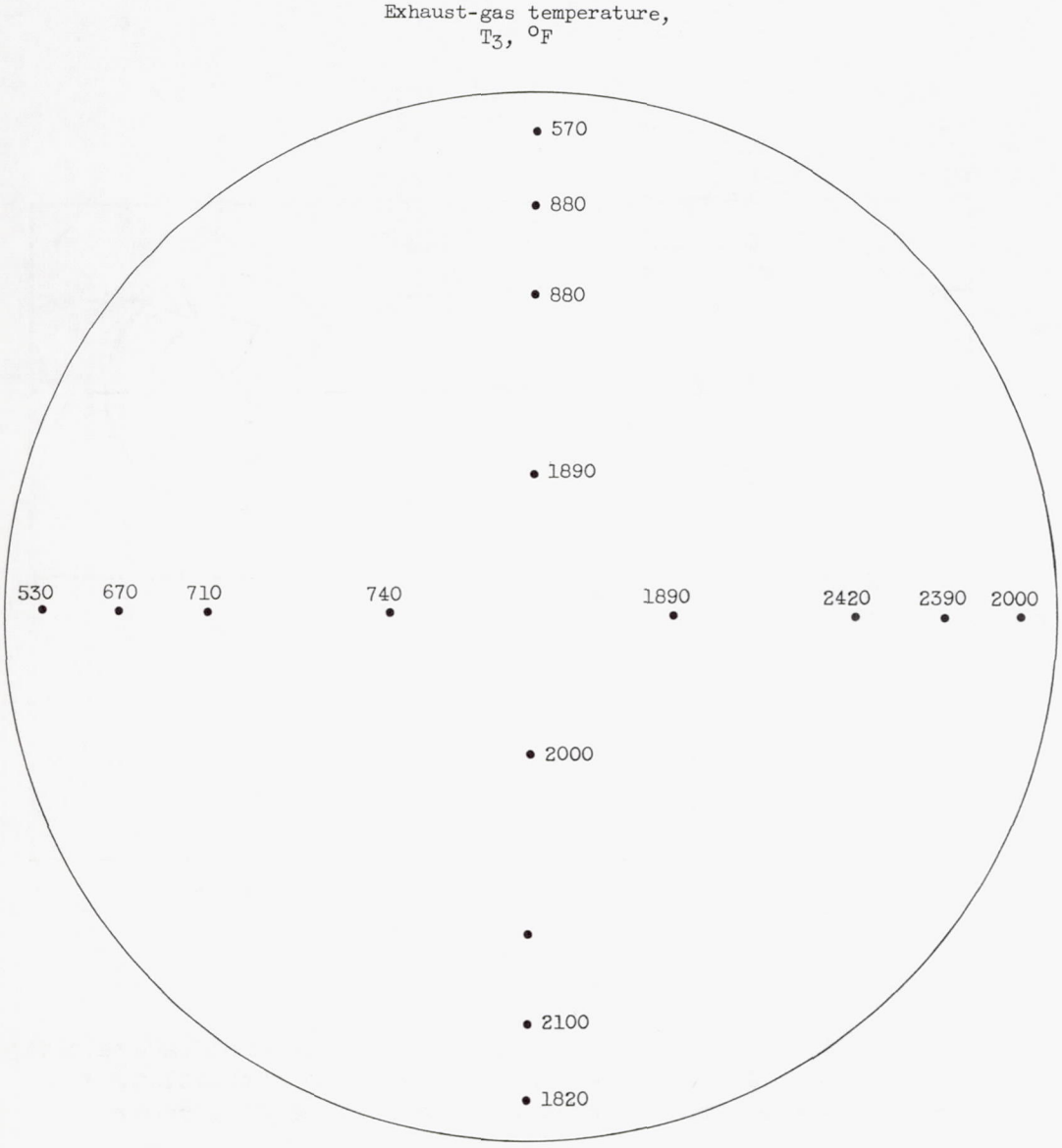
Figure 9. - Combustor-inlet circumferential velocity profiles for configurations B and C with no combustion. Combustor-inlet static pressure, 35±6 inches of mercury absolute.



(b) Station 2.

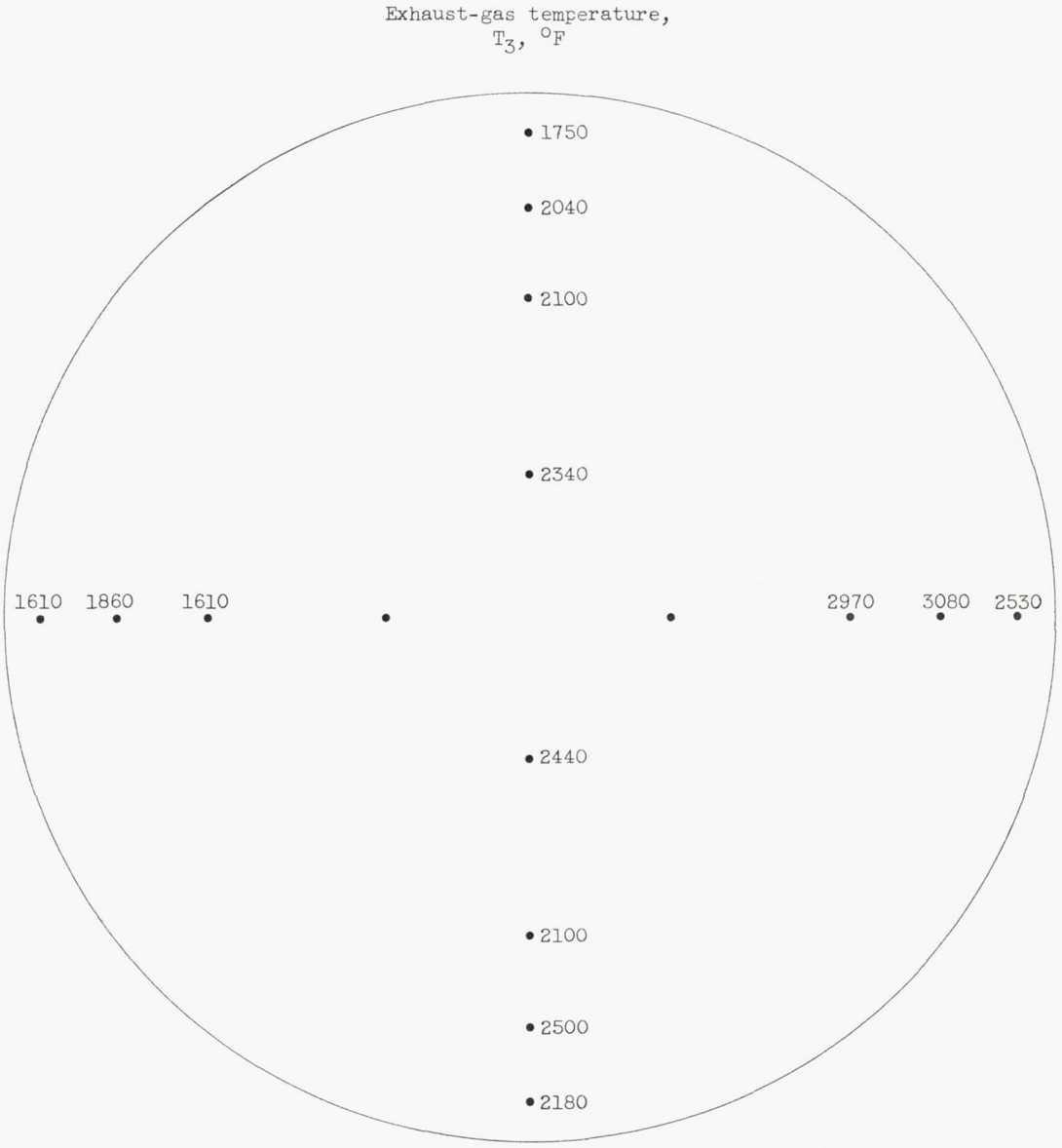
Figure 9. - Concluded. Combustor-inlet circumferential velocity profiles for configurations B and C with no combustion. Combustor-inlet static pressure, 35±6 inches of mercury absolute.

DECLASSIFIED



(a) Configuration A; equivalence ratio, 0.105; average combustor-exit temperature, 1440° F.

Figure 10. - Exhaust-gas temperature profile at station 3.

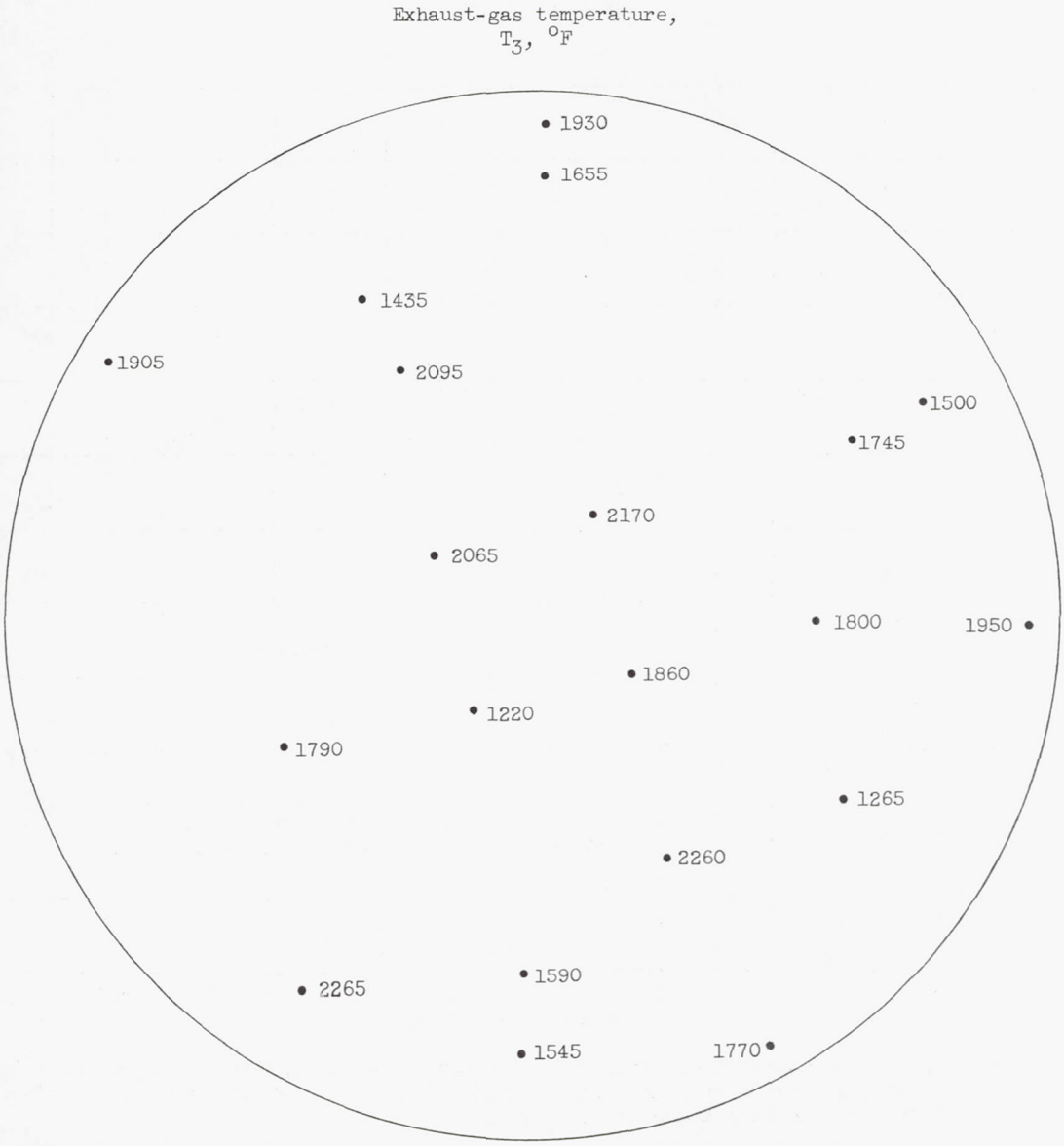


(b) Configuration A; equivalence ratio, 0.237; average combustor-exit temperature, 2220° F.

Figure 10. - Continued. Exhaust-gas temperature profile at station 3.

DECLASSIFIED

4232



(c) Configuration B; equivalence ratio, 0.225; average combustor-exit temperature, 1820° F.

Figure 10. - Concluded. Exhaust-gas temperature profile at station 3.

4232

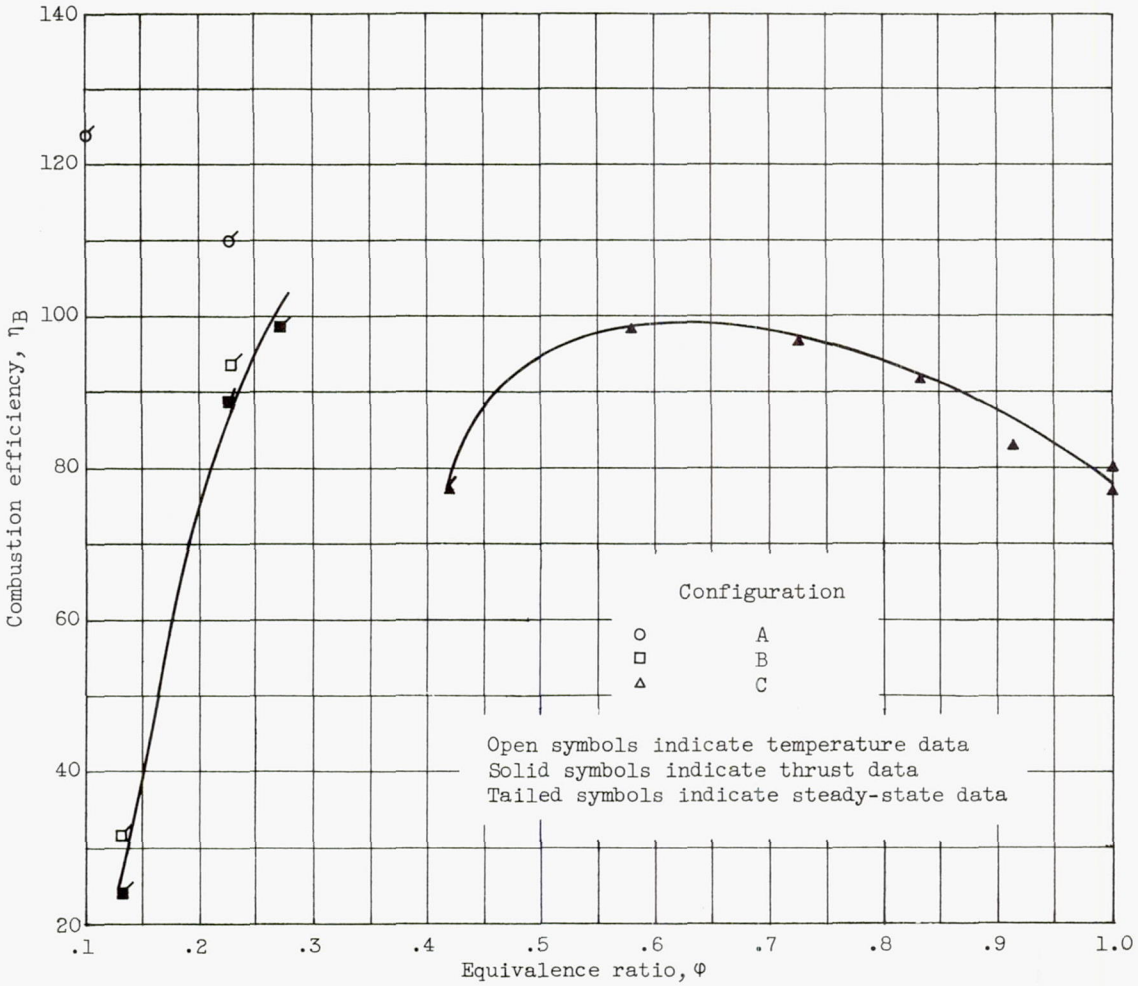


Figure 11. - Combustion efficiency of configurations A, B, and C. Combustor-inlet conditions: static pressure, 35±6 inches of mercury absolute; velocity, 230 to 270 feet per second; temperature, 220°±10° F.

DECLASSIFIED

4232

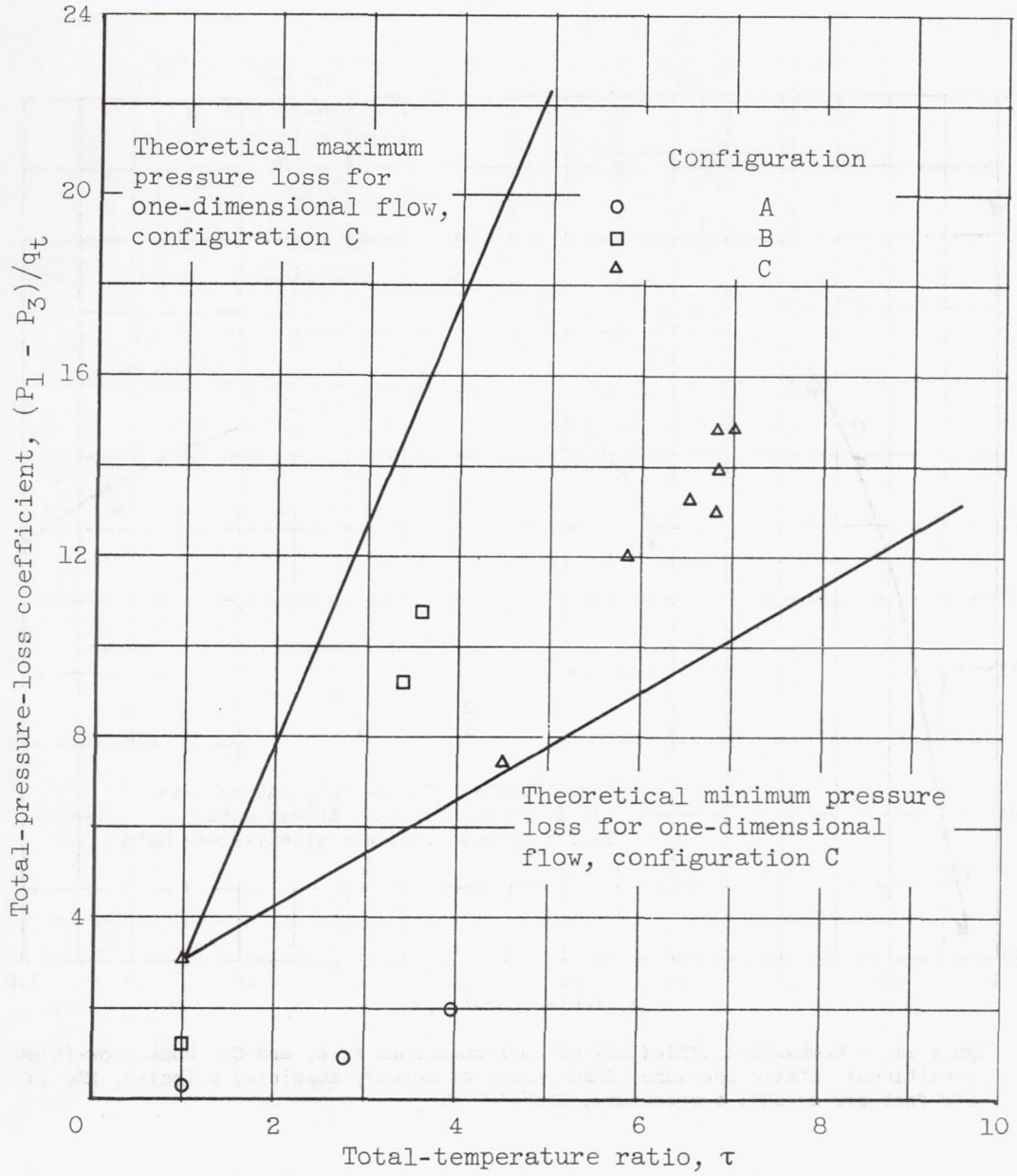


Figure 12. - Total-pressure loss for configurations A, B, and C. Combustor-inlet conditions: static pressure, 35±6 inches of mercury absolute; velocity, 230 to 270 feet per second; temperature, 220°±10° F.

4232

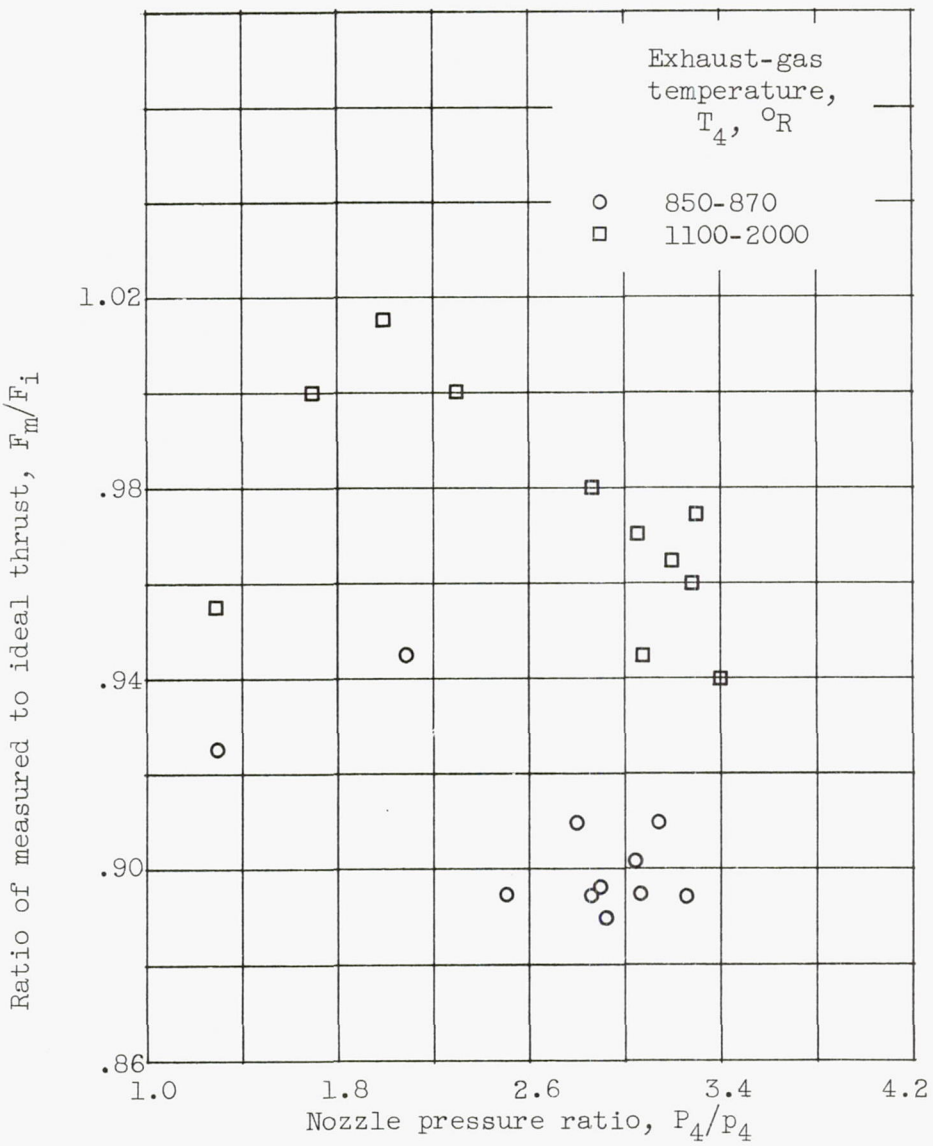
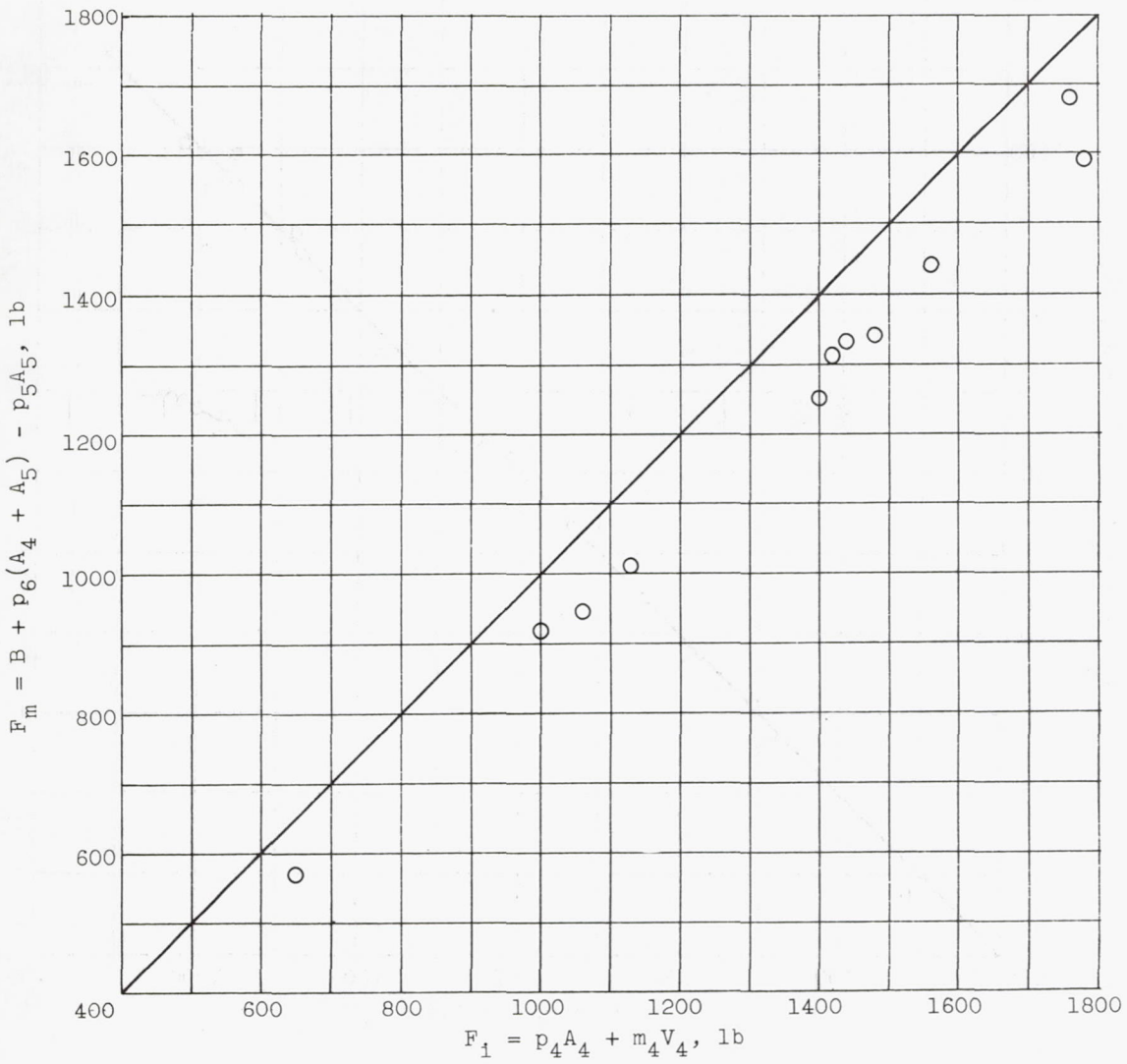


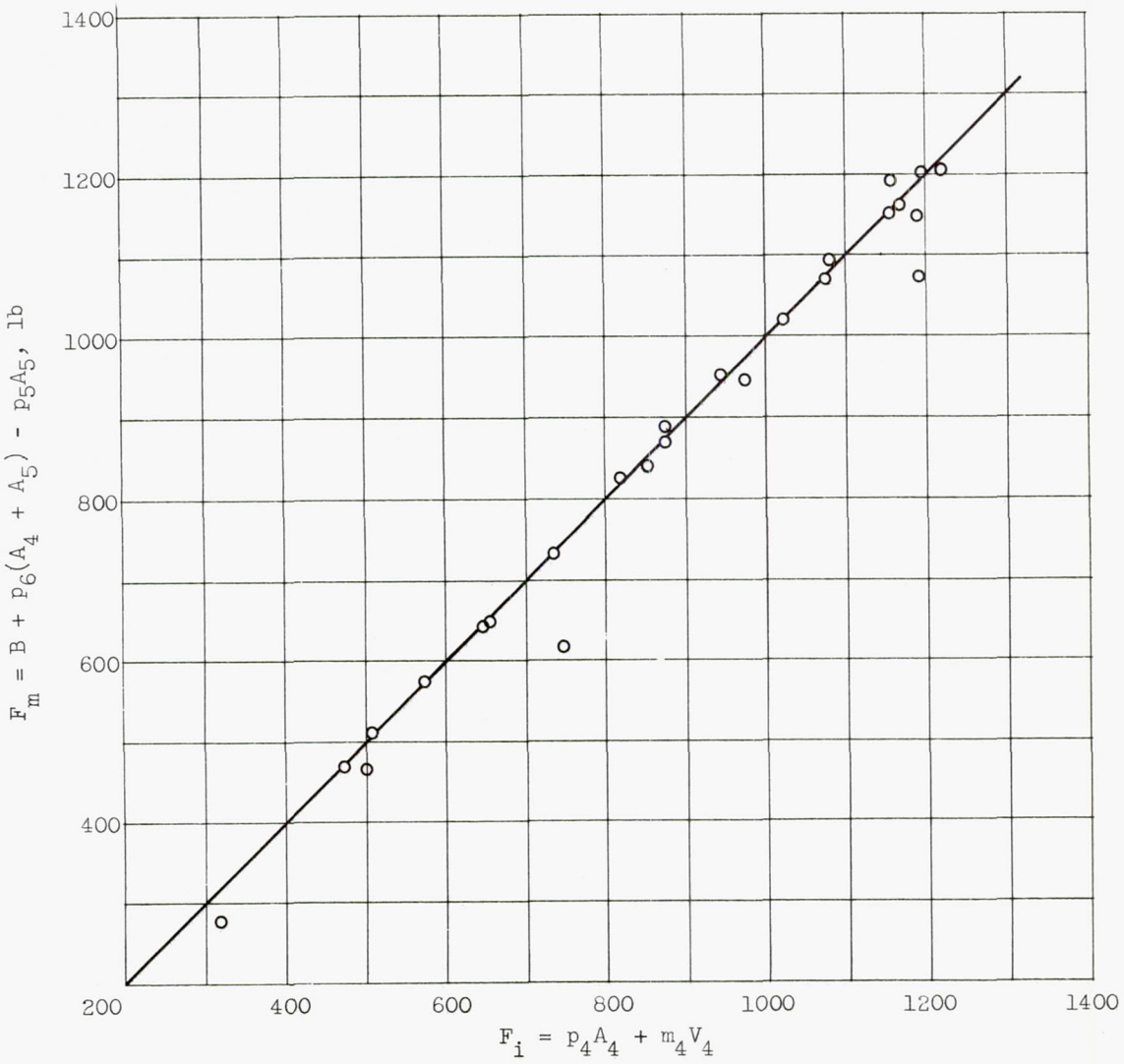
Figure 13. - Ratio of measured to ideal thrust for convergent-divergent nozzle (configuration A).

DECLASSIFIED



(a) Convergent-divergent exhaust nozzle (configuration A).

Figure 14. - Calibration of thrust barrel.



(b) Convergent exhaust nozzle (configurations B and C).

Figure 14. - Concluded. Calibration of thrust barrel.

UNCLASSIFIED

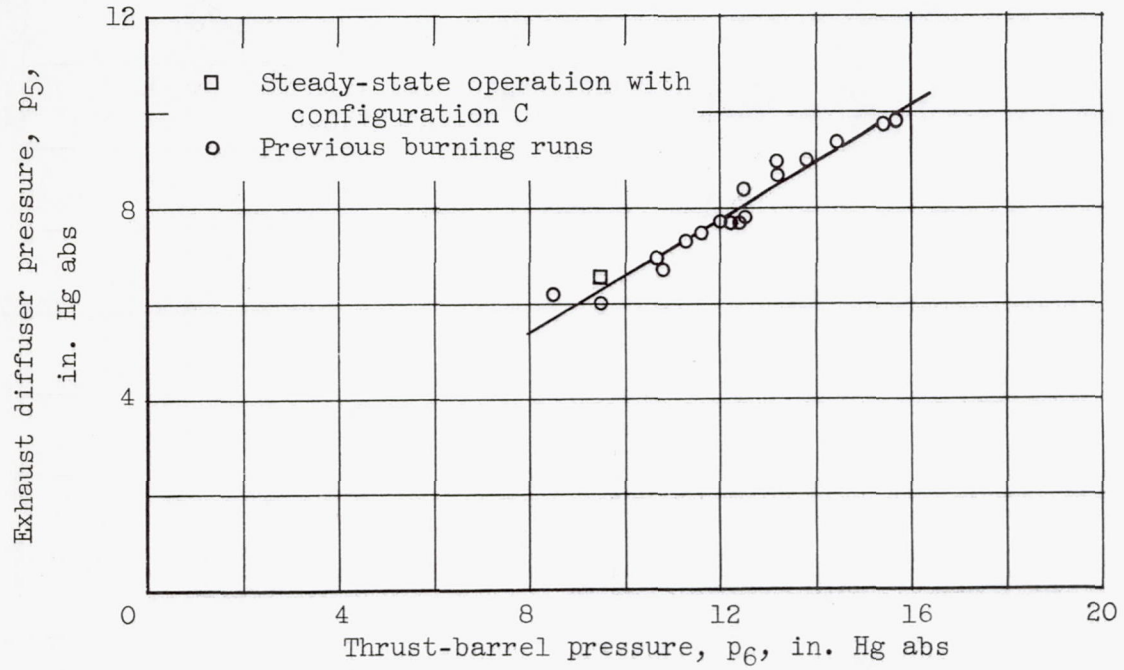


Figure 15. - Correlation of exhaust diffuser pressure with thrust-barrel pressure.

NACA - Langley Field, Va.